

DISS. ETH NO. TO BE INSERTED

- TOWARDS VESTIBULAR IMPLANTS -
EFFECTIVE PULSE MODULATION IN HUMAN
PATIENTS AND ELECTRICALLY EVOKED COMPOUND
ACTION POTENTIALS IN ANIMAL MODELS

A dissertation submitted to
ETH ZURICH

for the degree of
DOCTOR OF SCIENCES

presented by
THUY ANH KHOA NGUYEN
Diplom-Ingenieur Mechatronik (TU Dresden)
born 18 August 1985
citizen of Germany

accepted on the recommendation of
Prof. Dr. Manfred Morari, examiner
Prof. Dr. Silvestro Micera, co-examiner
Dr. Barry Seemungal, co-examiner

2015

ABSTRACT

Every day we use our five senses to interact with our environment. A sixth sense – the sense of balance – helps us navigate and orient through this environment. The vestibular system is the main contributor to this sense. Its sensory organs are located in the inner ear. Bilateral loss of vestibular sensation (BVL) is severely debilitating and significantly reduces quality of life. Affected patients have currently no effective treatment option and a vestibular implant (VI) might be the most promising option.

The field of vestibular implant research is entering an exciting period. More than a decade of animal work is now being translated to human patients and studies with patients are surging forward. With several collaborators within the EU and US project CLONS, we made further inroads towards a commercial VI.

In the first part of this thesis, we developed a real-time research platform to investigate pulse rate and pulse amplitude modulation. These two modulation paradigms were then tested in four BVL patients which were instrumented with modified cochlear implants for vestibular stimulation. Our results strongly support pulse amplitude modulation as stimulation paradigm for implant activation because it evoked significantly stronger eye movement responses. Furthermore, a model of the eye movement reflex pathway provided insights into how differently the two modulation paradigms engage vestibular afferents. Future experiments should investigate how the performance of these modulation paradigms changes with continuous stimulation as animal research suggests improvements in eye movement response over time.

In the second part of the thesis, we lay the groundwork to pursue the goal of a closed-loop VI that could boost implant performance. We adapted artifact reduction techniques to record vestibular electrically evoked compound action potentials with a custom electrode array. We then correlated these compound potentials to eye movement responses for different stimulation scenarios that would resemble the operating mode of a VI. Our results showed a (piecewise) linear pattern that could be used clinically for implant fitting (i. e. identification of stimulation thresholds). Our results also showed that utilization of these compound potentials as feedback signal in a closed-loop VI may be feasible and requires further work.

ZUSAMMENFASSUNG

Wir nutzen täglich unsere fünf Sinne, um mit unserer Umgebung zu interagieren. Unser sechster Sinn – der Gleichgewichtssinn – hilft, dass wir uns in dieser Umgebung navigieren und orientieren können. Das Vestibulärsystem trägt massgebend dazu bei. Ein beidseitiger Verlust des Vestibulärfunktion ist eine schwerwiegende Behinderung und mindert nachweislich die Lebensqualität. Betroffene Patienten hatten jedoch bisher keine Therapiemöglichkeit. Ein Vestibulärimplantat (VI) ist ihre grösste Chance.

Das Forschungsfeld der VI-Forschung steht vor einer spannenden Phase. Mehr als zehn Jahre Forschung an Tieren wird derzeit auf menschliche Patienten übertragen und Studien mit Patienten nehmen zu. Im Rahmen des EU-US Projekts CLONS, machten wir mit unseren Projektpartnern weitere Fortschritte bzgl. eines Vestibulärimplantats.

Im ersten Teil der Dissertation entwickelten wir eine Echtzeitplattform, um Pulsraten- und Pulsweitenmodulation für ein VI in Patienten zu untersuchen. Die Patienten hatten bereits ein modifiziertes Cochlearimplantat erhalten, das Elektroden zur elektrischen Stimulierung des Vestibularnervs enthielt. Unsere Ergebnisse zeigten deutlich, dass Pulsamplitudenmodulation in akuten Tests stärkere Augenbewegungen auslöste als Pulsratenmodulation und daher beim erstmaligen Einschalten des Implantats ausgewählt werden sollte. Unser Modell deckte überdies auf, wie die beiden Modulationstechniken Vestibularneuronen aktiviert. Zukünftige Experimente müssen klären, ob und um wieviel sich die Performanzen der beiden Modulationsarten bei chronischer Stimulierung ändern. Literatur legt nahe, dass sich Augenbewegungen verstärken würden.

Im zweiten Teil der Dissertation legten wir den Grundstein für die Entwicklung einer Regelschleife für ein VI, welche die Leistung des Implantats weiter steigern könnte. Techniken zur Artefaktreduzierung wurden modifiziert, um vestibuläre evozierte Potenziale mit einem doppelseitigen Elektrodenarray zu messen (VECAPs). Wir korrelierten diese VECAPs mit den durch elektrische Stimulierung ausgelösten Augenbewegungen. Die Ergebnisse zeigten für ein Szenario ein stückweises, lineares Muster, das zur Schwellwertbestimmung für das Implantat verwendet werden könnte. Außerdem zeigen unsere Resultate, dass VECAP potenziell rückführende Regelgrösse sein könnte für ein VI mit Regelkreis. Jedoch ist weitere Forschung dafür nötig.

PUBLICATIONS

The following publications are included in parts or in an extended version in this thesis:

Part I

- Nguyen TAK, Ranieri M, DiGiovanna J, Peter O, Genovese V, Perez Fornos A, and Micera S. A Real-Time Research Platform to Study Vestibular Implants With Gyroscopic Inputs in Vestibular Deficient Subjects. *Biomedical Circuits and Systems, IEEE Transactions on* 8: 474-484, 2014.
- Nguyen TAK, DiGiovanna J, Cavuscens S, Ranieri M, van de Berg R, Guinand N, Carpaneto J, Kingma H, Guyot JP, Micera S, Pérez-Fornos A. Pulse Amplitude Modulation Is More Effective Than Pulse Rate Modulation during Acute Electrical Stimulation with a Vestibular Implant in Human Patients. *Brain (in preparation)*, 2015.

Part II

- Nguyen TAK, DiGiovanna J, Merfeld D, and Micera S. Comparing Artifact Reduction Methods for Recording Vestibular Evoked Potentials in a Vestibular Neuroprosthesis. In: 34th Annual International Conference of the EMBS. San Diego, CA: 2012.
- Nguyen TAK, Gong W, DiGiovanna J, Poppendieck W, and Micera S. Investigating Vestibular Evoked Potentials as Feedback Signal in a Vestibular Neuroprosthesis: Relation to Eye Movement Velocity. In: *Converging Clinical and Engineering Research on Neurorehabilitation*, edited by Pons JL, Torricelli D, and Pajaro M. Springer Berlin Heidelberg, 2013a, p. 1325-1329.
- Nguyen TAK, Gong W, Poppendieck W, DiGiovanna J, and Micera S. Investigating ocular movements and Vestibular Evoked Potentials for a vestibular neuroprosthesis: Response to pulse trains and baseline stimulation. In: 2013 6th International IEEE/EMBS Conference on Neural Engineering (NER). San Diego, CA, USA: 2013b.
- Nguyen TAK, DiGiovanna J, Gong W, Haburcakova C, Poppendieck W, Micera S, Merfeld D. Characterizing Vestibular Electrically Evoked Compound Action Potentials in Guinea Pigs. In: 38th Annual MidWinter

Meeting of the Association for Research in Otolaryngology. Baltimore, MD, USA, 2015.

Furthermore, the following publications were part of my PhD research, are however not covered in this thesis. The first two publications were early animal recordings with a setup different from the one used in the main section. The topics of the other two publications are outside of the scope of the material covered here:

- Kögler V, Nguyen TAK, DiGiovanna J, and Micera S. Recording Vestibular Evoked Potentials Induced by Electrical Stimulation of the Horizontal Semicircular Canal in Guinea Pig. In: IEEE EMBS Conference on Neural Engineering. Cancun: 2011.
- Nguyen TAK, Kögler V, DiGiovanna J, and Micera S. Finding Physiological Responses in Vestibular Evoked Potentials. In: IEEE Engineering in Medicine and Biology Conference. Boston, MA, USA: 2011.
- Poppendieck W, Sossalla A, Krob M-O, Welsch C, Nguyen TAK, Gong W, DiGiovanna J, Micera S, Merfeld D, and Hoffmann K-P. Development, manufacturing and application of double-sided flexible implantable microelectrodes. Biomedical Microdevices 1-14, 2014.
- Van De Berg R, Guinand N, Nguyen TAK, Ranieri M, Cavuscens S, Guyot J-P, Stokroos R, Kingma H, and Perez Fornos A. The vestibular implant: Frequency-dependency of the electrically evoked Vestibulo-Ocular Reflex in humans. Frontiers in Systems Neuroscience 8: 2015.

ACKNOWLEDGMENTS

During my graduate studies, I had the opportunity to work in Zurich, Lausanne, Geneva, Maastricht and Boston where I met so many great and inspiring people. I am thankful to all of them and I appreciated having met and worked with them.

I want to especially thank Jack DiGiovanna, PhD, Prof. Micera, and Prof. Morari for their support and supervision as well as helping me to grow as researcher. Thank you also, Dr. Seemungal, for being on my committee.

Now a list of thank you, danke, merci and grazie. You guys are amazing and made this wonderful!

EPFL Elvira, Martina, Sophie, Jenifer, Jennifer, Anouk, Eduardo, MarcoB, MarcoC, Stani, Francesco, Andrea, Edoardo, Emmanuele, Steven, Christian P

ETHZ Claudia, Robert, Joe, Marco, Stefan, Stephan, Peter, Nikos, Tyler, Sean, Gemma, Xavier, Alex, RoboCup students, Prof. Lygeros

HUG Angélica, Maurizio, Samuel, Nils, Prof. Guyot

AZM Raymond, Pascal, Rene, Prof. Kingma

MEEI Csilla, Fauzia, Saori, Lara, Wangsong, Ryan, Prof. Merfeld

- Philipp V, Istvan, Tri, 25 Dover St, Cambridge, MA (AnneMarie, Christina, Rafael, Matt, Ray), Silvia, Xio, Darryl, Reyk, Inesa, Jakob, Jan, Sven

And last, but certainly not least, my family. My parents and brother have blessed me with endless love. Cam on.

CONTENTS

1	INTRODUCTION	1
2	BACKGROUND	5
2.1	Structure and Physiology of the Vestibular System	5
2.2	Vestibular Implant Development	9
I ASSESSING PULSE AMPLITUDE AND PULSE RATE MODULATION IN INSTRUMENTED BVL PATIENTS		17
3	REAL-TIME RESEARCH PLATFORM FOR HUMAN VESTIBULAR IMPLANTS	19
3.1	Introduction	19
3.2	System Architecture	21
3.3	Results	31
3.4	Discussion	35
3.5	Summary	41
4	EFFECTS OF PULSE AMPLITUDE AND PULSE RATE MODULATION DURING ACUTE ELECTRICAL STIMULATION WITH A VESTIBU- LAR IMPLANT IN HUMAN PATIENTS	43
4.1	Introduction	43
4.2	Methods	44
4.3	Results	48
4.4	Discussion	51
4.5	Summary	54
	Appendices	55
II VECAP – VESTIBULAR ELECTRICALLY EVOKED COMPOUND AC- TION POTENTIAL		59
5	ARTIFACT REDUCTION FOR VECAP MEASUREMENT	61
5.1	Introduction	61
5.2	Methods	62
5.3	Results	66
5.4	Discussion	68
5.5	Summary	71
6	INVESTIGATING VECAP AND VOR CORRELATION	73
6.1	Introduction	73
6.2	Materials	74

CONTENTS

6.3 Results	77
6.4 Discussion	80
6.5 Summary	84
III CONCLUSIONS	87
7 SUMMARY AND OUTLOOK	89
BIBLIOGRAPHY	93
ACRONYMS	99
CURRICULUM VITAE	101

LIST OF FIGURES

Figure 2.1	Anatomy and physiology of the vestibular labyrinth	6
Figure 2.2	Concept of vestibular implant	12
Figure 3.1	CompactRIO system overview and user interface	22
Figure 3.2	CompactRIO interconnection and signal flow	26
Figure 3.3	CompactRIO flow charts for GUIs 3, 4	27
Figure 3.4	CompactRIO response times	32
Figure 3.5	CompactRIO function modulation	33
Figure 3.6	CompactRIO gyroscope modulation	36
Figure 4.1	Charge-equivalent PAM, PRM and VOR model	47
Figure 4.2	Average peak eye velocities to PAM and PRM	49
Figure 4.3	Eye movement response axes to PAM and PRM	50
Figure 4.4	Simulations result with vestibular nuclei model	52
Figure 5.1	Setup for VECAP recording	64
Figure 5.2	Monopolar and bipolar stimulation and recording	67
Figure 5.3	Effect of phase width on recording	67
Figure 5.4	Artifact reduction for VECAP recording	69
Figure 6.1	Closed-loop VI concept for a vestibular implant and VECAP test paradigm	76
Figure 6.2	VECAP-VOR correlation to single pulses	78
Figure 6.3	VECAP-VOR correlation to pulse trains	80
Figure 6.4	VECAP-VOR correlation with baseline stimulation	81

LIST OF TABLES

Table 3.1	Settings for CRIo validation	31
Table 3.2	Statistics for CRIo function modulation	34
Table 3.3	Statistics for CRIo gyroscope modulation	34
Table 4.1	Patient demographics and stimulation parameters	55
Table 6.1	Stimulation and recording settings for VECAP-VOR study	77

1

INTRODUCTION

The senses do not err — not because they always judge rightly, but because they do not judge at all.

Critique of Pure Reason, Immanuel Kant, 1781

Vision, touch, taste, hearing and smell are the five senses that Aristotle (384 BC - 322 BC) is believed to have originally classified. The notion of a sixth sense consisting of the vestibular and other proprioceptive systems emerged only after the mid-19th century, when scientists realized that vestibular organs in the inner ear were not related to hearing, but involved in equilibrium functions. Today, we are more aware of the vestibular system's instrumental role in our everyday life.

Each of our inner ears is equipped with five organs to sense head movement. Three semicircular canals sense head rotation and two otolith organs sense head translation. A disruption of their inputs can deteriorate motor coordination, postural control and spatial orientation. While individuals with unilateral vestibular deficiency or mild and moderate bilateral vestibular deficiency can at least partially compensate, patients with bilateral vestibular loss (BVL) have currently no viable treatment option. They can experience chronic dizziness, vertigo, imbalance or oscillopsia (blurred vision), thus significantly reducing their quality of life (Sun et al., 2014; Guinand et al., 2012a).

Guinand et al. (2012a) estimated the prevalence of BVL at 81 in 100'000 people, or 500'000 patients in Europe and the USA, three million worldwide. Though this number is considerably smaller than, for instance, for deaf people (approx. 70 million worldwide), BVL results in significant economic and social burdens, therefore warranting the development of a vestibular implant (VI) to restore vestibular function.

TOWARDS VESTIBULAR IMPLANTS

VIIs are conceptually similar to cochlear implants (CI) which restore auditory function. CIs have been the most successful neuroprosthesis to date with more than 300'000 people implanted worldwide (NIH report 2013). In a VI,

INTRODUCTION

electrodes or electrode arrays are placed in the peripheral vestibular nerve branches to apply electrical stimulation with the goal to convey information about head movement to the vestibular system.

Electrical stimulation of vestibular organs was first demonstrated in the 1960s. Suzuki, Cohen and colleagues activated vestibular structures with implanted wire electrodes in cats as well as monkeys (Cohen and Suzuki, 1963; Suzuki et al., 1969). The stimulation induced eye movement – evidence of Vestibular-Ocular Reflex (VOR) activation. A healthy VOR contributes significantly to gaze stabilization and has been commonly regarded as the best objective measure of vestibular function.

In 2000, Gong and Merfeld succeeded in building the first self-contained, one-dimensional VI in a guinea pig (Gong and Merfeld, 2000). Their approach was then extended to cover all three rotational axes in chinchillas (Della Santina et al., 2007). The viability of a VI in human patients was demonstrated by Guyot and colleagues (Guyot et al., 2011ab).

In 2009, the Automatic Control Laboratory at ETH Zurich and several partners¹ started a four year project to pursue an innovative closed-loop neural prosthesis for vestibular disorders (CLONS). One ambition was to develop stimulation strategies to boost implant performance and aid neuroplasticity. The latter term generally describes the brain's (impressive) ability to adapt to changes in e.g., behavior, neural processes or environment. In several studies, animal subjects acclimated to continuous vestibular stimulation and showed improved responses with time that were attributed to plasticity (e.g., Merfeld et al., 2007, Dai et al., 2011). A closed-loop VI would hold promise to potentially accelerate plasticity and to enhance responses even further.

With several project partners, we began laying the groundwork for a closed-loop VI. Such a device would require a more immediate feedback signal than the naturally occurring visual feedback. The VOR typically has a latency of 5-10 ms (Aw et al., 1996). To explore potential feedback signals, collaborators designed and implanted a double-sided electrode arrays in guinea pigs (Poppendieck et al., 2014). A total of eight electrode sites facilitated both stimulation and recording of the peripheral vestibular nerve. With those arrays we identified vestibular electrically evoked compound action potentials (VECAPs,

¹ Partners were: Scuola Superiore Sant'Anna, Fraunhofer Institute for Biomedical Engineering, University College of London, Centre National de la Recherche Scientifique, Hôpitaux Universitaires de Genève, Massachusetts Eye and Ear Infirmary, ETH Zurich, and from 2010 also Med-El. With the appointment of Prof. Micera to EPFL Lausanne in 2011, work was transferred from Zurich to Lausanne.

pronounced vee-e-kaps) as potential feedback signal and investigated it in relation to eye movement responses in guinea pigs.

In a concurrent line of research, CLONS collaborators instrumented BVL patients, that also suffered from severe hearing loss, with hybrid cochlear-vestibular implants. These were modified CIs with nine electrode sites for cochlear and three electrode sites for vestibular stimulation. This approach provided established and approved CI technology as a possible fast-track to a commercial VI. However, it brought to focus the question of which stimulation paradigm was more effective: pulse amplitude (PAM) or pulse rate modulation (PRM). Goldberg and Fernandez' seminal studies found that primary afferents in the semicircular canals naturally encode information with spike rate modulation (Goldberg and Fernandez, 1971ab). This has been predominantly emulated with PRM in animal models. In contrast, stimulation strategies in CIs commonly employ PAM (Wilson et al., 2006). To compare both paradigms we tested them in four instrumented BVL patients during acute trials and strongly recommend PAM for the first time activation of a VI.

LAYOUT OF THIS THESIS

This thesis focuses exclusively on VIs that aim to restore vestibular function through electrical stimulation, specifically the replacement of semicircular canal function to sense head rotation. Other approaches to restore vestibular sensation such as sensory substitution (Wall et al., 2009), infra-red stimulation (Harris et al., 2009), transcutaneous galvanic stimulation (Cohen et al., 2012), cell- or gene-based research to regrow or repair sensory cells (e.g., Koehler et al., 2013) are not discussed herein because of their limited or (still) uncertain prospects compared to electrical stimulation.

The thesis details the author's contributions towards two aims: **Aim 1** identifying the more efficient electrical stimulation paradigm for initial VI activation in human patients, and **Aim 2** characterizing VECAPs in an animal model for a closed-loop VI that could potentially improve implant performance.

Following this introduction, Chapter 2 provides an overview of vestibular neurophysiology and VI research that has seen steady and promising progress over the last 15 years.

Part I presents the acute stimulation trials to investigate PAM and PRM stimulation paradigms in BVL patients. To this end, a customized real-time platform was programmed and deployed, described in Chapter 3. Experimental results and an accompanying neural network model are presented and discussed in Chapter 4.

INTRODUCTION

In Part II, Chapter 5 reports how to reduce stimulation artifact to measure VECAP. Chapter 6 presents VECAP characterization for single electrical pulses, pulse trains and continuous electrical stimulation and how VECAP correlated with VOR responses in guinea pigs.

Part III discusses the universal themes emerging from animal and human testing. Finally, an outlook suggests the critical research questions that have to be addressed for VIs to become a success.

BACKGROUND

We begin this chapter with a review of basic vestibular neurophysiology. More general and comprehensive vestibular neurophysiology is covered at length in *The Vestibular System: A Sixth Sense* (Goldberg et al., 2012) or *Clinical Neurophysiology of the Vestibular System* (Baloh and Kerber, 2011).

We then introduce the general VI design and describe its components such as motion sensor, electrodes and stimulation paradigms. For detailed reviews on the VI topic, see van de Berg (2011), Merfeld and Lewis (2012), or Fridman and Della Santina (2012). Readers familiar with semicircular canals, the vestibulo-ocular reflex and the VI concept may refresh on individual topics or view this chapter as reference.

2.1 STRUCTURE AND PHYSIOLOGY OF THE VESTIBULAR SYSTEM

Our peripheral vestibular system in the inner ear is a marvelous inertial sensor with a large dynamic range and high sensitivity. Figure 2.1A shows the division into outer, middle and inner ear. The latter consists of the membranous labyrinth that is contained within the bony labyrinth. The membranous labyrinth is filled with endolymph, an extracellular fluid with a distinctive, potassium-rich composition. It contributes to mechanotransduction, i. e. the conversion of head movement into nerve signals.

The membranous labyrinth includes the cochlea for hearing and also the five vestibular end organs for head movement sensing: the three semicircular canals (SCC) for head rotation and the two otolith organs, the utricle and saccule, for head translation. The three SCCs – horizontal, anterior and posterior – are named after their shape and position. Horizontal and superior canals are also called lateral and superior canals, respectively. Each SCC has an enlargement, the ampulla, containing the cupula, crista, sensory hair cells and innervating nerve fibers (Fig. 2.1B).

There are type I and type II hair cells (Fernandez et al., 1988a). Both types are innervated by afferent neurons, cells that transmit nerve signals to the central nervous system and efferent neurons, cells that receive nerve signals from the central nervous system. The afferent neurons' cell bodies are inside the vestibular or Scarpa's ganglion (named after Italian anatomist Antonio

BACKGROUND

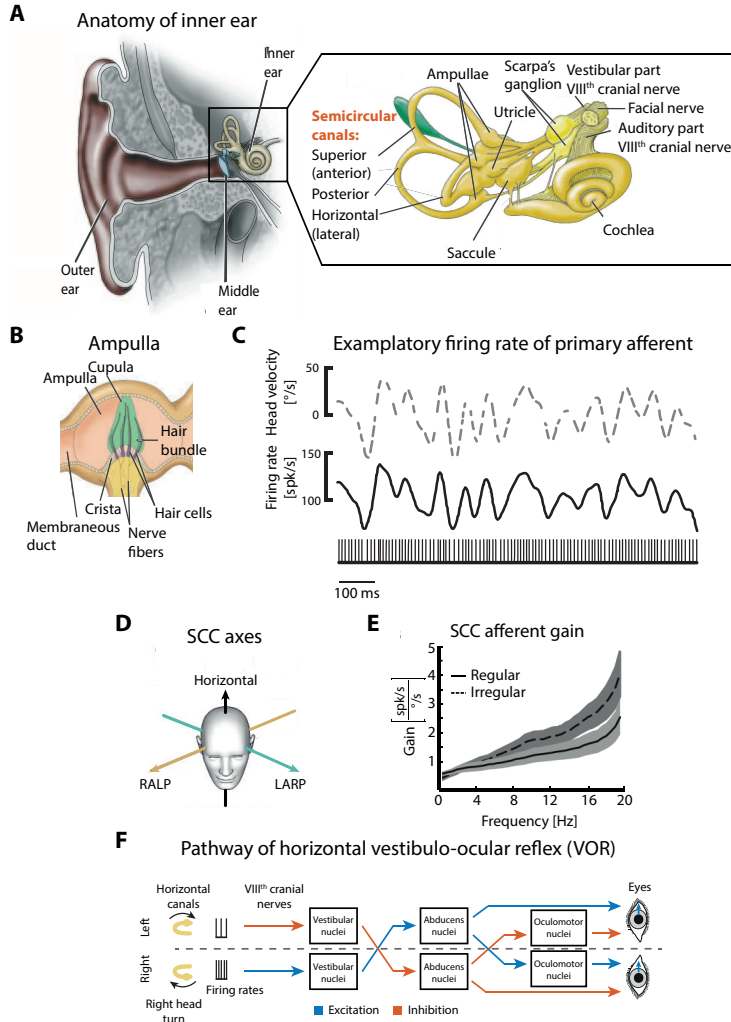


Figure 2.1: Anatomy and physiology of the vestibular labyrinth. (A) Anatomy of the ear with a close-up of the inner ear with its vestibular and auditory organs. (B) Each semicircular canal has an ampulla with the shown elements. In case of a rotation, the endolymph inside the canal deflects the cupula and triggers a change in firing rates of nerve fibers. (C) An example of how one afferent changes firing rate to head velocity. Note that at zero velocity, the afferent still has a resting discharge rate of approx. 90 spk/s. (D) The semicircular canals in both ears form pairs in three distinct axes: horizontal, LARP and RALP. (E) Regular and irregular afferents have different gains. Irregular afferents are more suited to encode high frequency movement. (F) The pathway of the horizontal VOR. A head turn to the right evokes excitation in the right horizontal SCC (firing rates increase) and inhibition in the left horizontal SCC. Through a three nuclei (or synapses) eyes respond with movement to the left to counter the head motion and stabilize gaze.

Scarpa). From there the vestibular nerve transmits information to and from the vestibular nuclei in the brainstem. Detailed accounts of these parts can be found elsewhere, e.g. The Vestibular System, Angelaki and Cullen (2008), Eatock (2011) or Cullen (2011).

Head movement mechanotransduction If the head is stationary, afferents in the SCC fire action potentials at a resting discharge rate, which in humans is typically 90 spikes per second (spk/s) (Goldberg and Fernandez, 1971a). This allows encoding of bi-directional rotation by increasing or decreasing the firing rate of afferents. For instance, a right head turn results in an increase (excitation) of afferent firing rate in the horizontal SCC of the right ear, whereas it leads to a decrease (inhibition) in the horizontal SCC of the left ear.

Specifically, the rotation is faithfully transmitted to the membranous labyrinth as it is fixed to the skull. However, the endolymph inside a SCC cannot follow the movement instantly due to its inertia and causes a deflection of the cupula. This induces a chain of biochemical events. Tiny deflections of hair bundles (100 nm) inside the cupula modulate ion currents and influences vestibular afferents, ultimately leading to excitation of the vestibular nerve in one ear (Fig. 2.1C) and inhibition of the vestibular nerve in the opposite ear. Movement transduction has a bandpass characteristic and is well adapted to encode head velocities over the natural frequency range (0.5-20 Hz, with peak around 2-5 Hz).

Excitation and inhibition have been described as the 'push-pull' mechanism of the vestibular system and provides some redundancy (which allows unilateral vestibular loss patients to compensate). Three pairs are formed: the two horizontal canals, left anterior and right posterior (LARP), and right anterior and left posterior (RALP). Each pair measures rotation along a single axis. Due to their orthogonality, they can provide the brain with a three-dimensional reconstruction of rotational motion (Fig. 2.1D).

Similarly, afferents in the otolith organs encode translational head motion. In contrast to the SCC, however, the utricle and saccule do not have distinct axes, but cover different directions. They additionally detect head tilt with respect to the earth's gravitational field.

Afferent properties Goldberg and Fernandez (1971a) classified two categories of afferents. At rest, *regular* afferents have relatively stable interspike intervals between action potentials, while *irregular* afferents have erratic intervals. This property is usually quantified with the normalized coefficient of variation cv^* , defined as the ratio of standard deviation of ISI over a standard mean interval

BACKGROUND

(in mammals 15 ms). These two afferent classes differ in various aspects. Here, we only highlight their response dynamics and electrical excitability.

Afferent response dynamics have been investigated in-vivo and with a torsion-pendulum model that models the fluid dynamics of the SCCs to calculate cupula deflection (Goldberg et al., 2012). Irregular afferents have higher sensitivity to rotational forces than regular afferents, while the latter have lower velocity detection thresholds. Irregular afferents best code high frequency movements. The movement transduction has a bandpass characteristic and is well adapted to encode head velocities over the natural frequency range (0.5-20 Hz, with peak around 2-5 Hz). Figure 2.1E shows the gain, i. e. change in afferent firing rate depending on head movement frequency. The mean maximum firing rate is approx. 500 spk/s, though some irregular afferents can briefly reach 1000 spk/s (Lysakowski et al., 1995).

With respect to electrical excitability, irregular afferents have lower thresholds, i. e. are more sensitive to electrical stimulation with galvanic currents than their regular counterparts (likely due to irregular afferents' thicker axons) (Goldberg et al., 1984).

Vestibulo-ocular reflex and optokinetic system The vestibulo-ocular reflex (VOR) is a reflexive eye movement that together with the optokinetic system (OKN) helps maintain a clear and stable view of the environment. Subjects with an impaired VOR have difficulty reading or recognizing objects while in motion. This impedes, for instance, independent driving. The reflex rotates our eyes in the opposite direction to any head motion and has both translational as well as rotational components. A head turn to the right causes excitation and inhibition of afferent firing rates of the right and left horizontal canals, respectively. This engages three nuclei and the oculomotor muscles to generate countering left eye movement (Fig. 2.1F). Because of its short pathway, often referred to as three neuron arc, the VOR is one of the fastest reflexes in our bodies with latencies between 5 and 10 ms.

For small head rotations (less than 15°), the VOR creates eye velocities matching head velocity. The VOR gain, the ratio of eye velocity over head velocity, in these cases equals 1. In these cases, the VOR has a predominantly linear behavior and has been described with linear control system tools (e.g., Robinson, 1981). For larger head movements, the VOR generates a nystagmus, a mixed strategy of slow and quick eye movements, to keep eye position within the oculomotor range.

Rotations solely around the horizontal axis result in predominantly horizontal VOR. Rotations along the LARP or RALP axis will yield vertical and also torsional VOR.

The OKN uses solely visual input to stabilize gaze and is driven by retinal slip, the relative motion of the visual world across the retina. Normally, OKN complements VOR at low-frequency head movements and produces an optokinetic nystagmus, i. e. slow compensatory and quick resetting eye movements.

Peripheral vestibular disorders Chronic bilateral vestibular loss can have traumatic, ototoxic, infectious, autoimmune or congenital causes. However, approximately half of the cases are idiopathic (Guinand et al., 2012a). The onset of BVL can be sudden, for instance following trauma, or gradually such as with the genetic disorder DFNA9 that leads to loss of auditory and vestibular function (Manolis et al., 1996).

In some clinical cases, antibiotics such as gentamicin can be used to treat vertigo attacks in Ménière's disease. But gentamicin is highly ototoxic. It leads to a loss of type I hair cells, renders type II hair cells insensitive to motion and also reduces resting discharge rates of afferents by 23% in chinchillas (Hirvonen et al., 2005).

2.2 VESTIBULAR IMPLANT DEVELOPMENT

In comparison to deaf patients, BVL patients have currently no adequate treatment option. A vestibular implant could restore vestibular function in these patients. Both the improvement in their quality of lives as well as the economic benefit for society (Sun et al., 2014) justify the development of a VI.

We focus on VIs that specifically aim to restore SCC function. As we have learned in the previous section, otolithic organs encode various directions, in contrast to the distinct axes of SCCs. Therefore, replacement of otolithic function is deemed considerably more challenging since electrical stimulation would be insufficiently specific and would create sensations with various directions due to current spread in the target organ. In fact, one study suggested that providing solely rotational (SCC) information through a VI could also help with deficient otolith function (Sun et al., 2011).

General concept A VI has to replace the process of mechanotransduction, that is, first, sensing head rotation and decomposing head velocities into the horizontal, LARP and RALP axes. Second, a controller has to compute

BACKGROUND

the stimulation settings and a stimulator applies electrical stimulation to electrodes implanted in the labyrinth. Figure 2.2A visualizes the concept in a block diagram.

Rotation sensor First VI prototypes employed single axis micro-electro-mechanical rotation sensors (Gong and Merfeld, 2000). These are devices similar to integrated circuits with dimensions between 20 µm and 1 mm and contain a processing and a sensor unit. The rotation sensors are typically based on the tuning forks or vibrating wheel, i. e. structures, that are actively oscillating (forks or wheel), are displaced in their default plane of motion due to external forces. This displacement is then used to gauge rotation.

Today's MEMS gyroscopes are smaller, yet sense rotation in three axes, have improved sensitivity and larger measurement range compared to the sensor Gong and Merfeld used in 2000. The main remaining challenge is power consumption. Even at rest, the sensing structures have to maintain oscillation, therefore drawing ca. 5 mA. In comparison, a triple-axis accelerometer to measure linear acceleration uses ca. 100 µA, a 50-fold difference. However, a network of accelerometers would not accurately measure rotation (Park and Hong 2011). Ongoing research is directed at developing SCC-inspired rotation sensors with microfluidics (Andreou et al., 2014) that would consume less energy.

The rotation sensor has been typically placed externally in a head cap in animal models. For human patients, external placement inside the ear canal or rigidly fixed on the skull has been proposed as well as implantation (Garnham et al., 2012). Compared to the microphone in cochlear implants, the rotation sensor for a VI has to be secured in place to have fixed measurement axes. A fast and accurate procedure can align sensor measurements with SCC axes (DiGiovanna et al., 2012).

Electrode design and surgical placement Electrodes were originally fashioned from twisted platinum wire with approx. 75 µm diameter and 200 µm length for guinea pigs (Gong and Merfeld, 2000). They distinguished between two configurations, *monopolar* stimulation with one site in the labyrinth and a return electrode in the animal's neck musculature. In contrast, *bipolar* stimulation would use an electrode inside the labyrinth as return electrode.

Learning from experience as well as three-dimensional modeling of the inner ear, customized electrode arrays were manufactured for better placement. The different electrode sites with controlled spacing allow for redundancy, and also acquisition of VECAPs (Chiang et al., 2011; Poppendieck et al., 2014).

Validation of these custom electrodes in humans would require substantial effort to obtain regulatory approval. Cochlear implants, on the other hand, offer established and approved electrode design and have up to 22 electrode sites. Thus, research groups have been adopting modified CIs that provide extra-cochlear electrode sites for vestibular stimulation (Perez-Fornos et al., 2014; Golub et al., 2013; Valentin et al., 2013).

Different approaches have been established for the surgical placement of the electrodes (van de Berg et al., 2012). In the intralabyrinthine approach, electrodes are inserted close to the cristae of the ampullae. This avoids an injury of the middle ear and reduces the probability of activating the facial nerve during stimulation. However, electrical stimulation of the ampullae may result in an insufficient response as the corresponding nerve dendrites (fibers) may have died back towards scarpa's ganglion. In the extralabyrinthine approach, Guyot and co-workers successfully placed an electrode not close to the ampullae, but in a depression drilled near the posterior ampillary nerve branch in one patient.

Vestibular implantation carries a considerable risk of hearing damage due the structure's proximity. Mild hearing loss occurred in rhesus monkeys (Dai et al., 2010) and some patients implanted with a VI suffered significant hearing impairment at the University of Washington (A. Perez-Fornos and N. Guinand, *pers. comm.*). In contrast, CLONS collaborators in Geneva and in Maastricht have been conservative and only selected BVL patients also suffering from deafness.

Electrode insertion in animal models often renders the subjects vestibular deficient. This is also referred to as canal plugging and restricts endolymph movement that deactivates SCC function. In another approach, ototoxic antibiotic gentamicin has been injected to eliminate vestibular sensation (Della Santina et al., 2007).

To facilitate notation of electrode placement, electrodes placed close to or into the lateral ampillary nerve are called *LAN*, for the superior and posterior ampillary nerves we will use *SAN* and *PAN*, respectively.

Stimulation paradigm Stimulation paradigms try to mimic the afferents' natural resting discharge rate and spike rate modulation. Specifically, electric pulses are applied with a baseline pulse rate and pulse rate modulation (PRM). To replicate the excitation and inhibition ('push-pull') mechanism of both ears, VIs should be ideally implanted bilaterally in BVL subjects. Bilateral implantation and stimulation has been reported for guinea pigs (Gong et al., 2008). However, due to the cost and risk of the surgery, instrumentation is

BACKGROUND

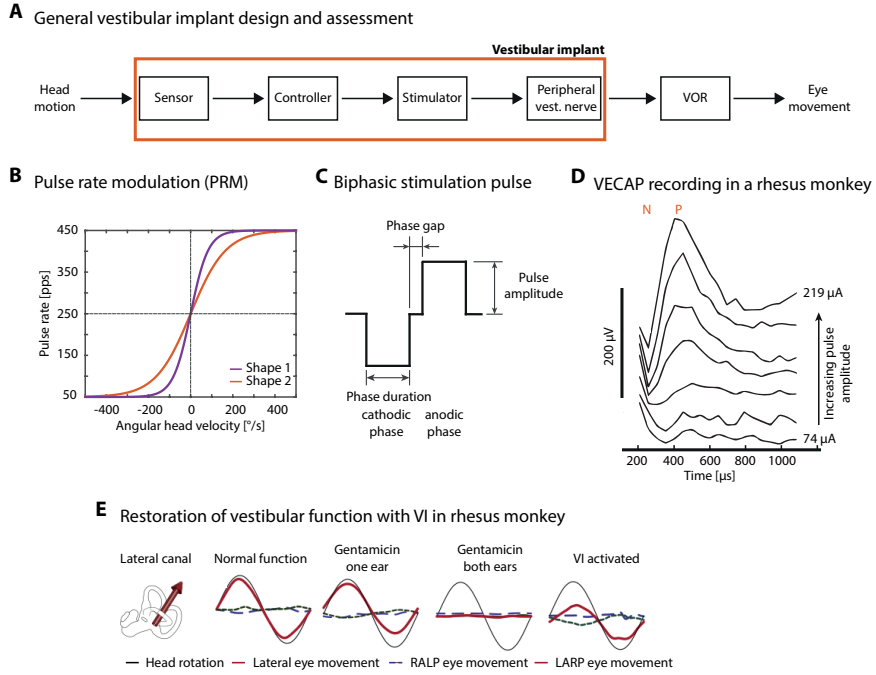


Figure 2.2: Concept of VI, stimulation paradigms and VECAPs. (A) The concept of current vestibular implants. Head motion is sensed by a sensor such as gyroscope and/or accelerometers. A controller dissects measurements into the three rotational axes horizontal, LARP and RALP and sends corresponding stimulation pulses to the stimulator that applies electrical stimulation to the peripheral vestibular nerve. The stimulation activates the VOR pathway and eye movement response is used as benchmark for stimulation efficacy. (B) Most VIs use pulse rate modulation modeled with an equation similar to Eq. 2.1. Two shapes are shown here, shape 1 would be more sensitive to velocities between -200 and 200 °/s than shape 2. (C) A VI uses biphasic, charge-balanced pulses with the parameters shown. (D) VECAPs from literature had characteristic negative (N) and positive waves (P). From Nie et al. (2011). (E) From Dai et al. (2011), an example of normal vestibular function in a rhesus monkey. Subsequently the researchers eliminated vestibular function with gentamicin and were able to restore it partially with the VI.

restricted to one ear at this stage of VI development. The rationale is to restore vestibular function to a level comparable to unilateral vestibular loss patients that can compensate well in everyday life for their deficiency.

To create balanced space for excitation and inhibition, the baseline pulse rate has been elevated to 200 or 250 pulses per second (pps). This would give equivalent range to increase the pulse rate to 500 pps (mean maximal natural firing rate 500 spk/s) or to decrease it to 0 pps. In case afferents had a natural resting discharge rate (e.g., 90 spk/s), that rate would be the lower bound. Note the difference in units: We use spk/s for afferents' natural and spontaneous firing rate, while pps is used for induced firing rate by electrical stimulation. Merfeld et al. (2007) used Eq. (2.1) for PRM, see also Fig. 2.2B.

$$pr = pr_{base} + pr_{range} \left[\tanh \left(\frac{\omega}{s_{shape}} \right) \right] \quad (2.1)$$

where pr is applied pulse rate, pr_{base} and pr_{range} the baseline pulse rate and range, respectively, ω the angular rate and s_{shape} is a shape factor and determines for instance the region of linearity.

Electric pulses are applied as biphasic, charge-balanced and symmetric pulses. This pulse shape avoids electrode corrosion and evolution of gas or other toxic substances at the metal-saline interface due to faradaic and oxidation-reduction reactions (Rose and Robblee, 1990; Merrill et al., 2005). The leading phase is usually the cathodic phase (negative current amplitude) as this has been shown to be more effective in generating action potentials. Figure 2.2C shows the biphasic pulse and its parameters.

Gong and Merfeld (2000) were guided by the original studies of Suzuki and Cohen in the 1960s and determined through trial and error a phase width and phase gap of 200 μ s. This has been typically used in animal models as well as patients. A comprehensive study by Davidovics et al. (2011) found that both PRM as well as pulse amplitude modulation (PAM) effectively elicited eye movement responses. They also varied phase width systematically. The group stated in that PRM with short pulse widths should be "the foundation for further optimization". This was later refined to endorse co-modulation of both pulse amplitude and pulse rate (Davidovics et al., 2012, 2013). They found that responses depended on baseline pulse rate with low value favoring PRM, while superphysiological baseline pulse rates favored PAM. Similarly, Guyot et al. used a high baseline pulse rate of 400 pps in instrumented patients and observed larger eye movement in response to PAM than PRM.

BACKGROUND

Assessment of VI performance The VOR response is regarded as the most objectively measured output of the vestibular system. In animal models, search coils are implanted into the eye(s) (Gong and Merfeld, 2000). In a controlled electromagnetic field eye movement, and thus coil movement, can be recorded to measure eye movement. Videooculography is another means and has been employed in animal models as well as human patients. A camera mounted on special glasses or placed in front of the subject and corresponding software track the pupil's movement. Coil measurements currently provide higher sampling rates (e.g., 1 kHz) and better resolution. However, placement of coils can lead to edema and trauma that may distort eye movements.

Since the vestibular system also contributes to perception and posture, VI performance should be evaluated not only through the VOR response. Squirrel and rhesus monkeys were trained to execute a subjective visual vertical task and a balance perturbation task (Thompson et al., 2012). In the first task, subjects are tilted in a dark environment and need to align a visual bar to what they perceive as earth-vertical. In the second task, subjects stood on a balance platform in their natural quadropedal stance with different support surfaces (e.g., rubber foam) or in a wide and narrow stance. However, these tasks required substantial training and testing time with animal subjects. Perceptual tasks might be therefore more conveniently performed with human patients.

VECAPs could be another objective metric of vestibular function. They are a measure of gross action potential activation generated in response to electrical stimulation by a population of nerve fibers. Historically, ECAPs were measured in the auditory nerve of CI users (Brown and Abbas 1990) to investigate their clinical utility (Abbas et al., 1999). Possible applications include threshold prediction and automatic CI fitting (i.e., optimizing stimulation parameters). Today it is used to help setting stimulation parameters in infants and children (McKay et al., 2013).

VECAPs have been first reported 2011 as tool for electrode placement during surgery (Nie et al., 2011) and some correlation with VOR responses has been demonstrated (Dai et al., 2012). Figure 2.2D shows an example with the characterisitc negative peak N and positive peak P (literature also uses the term wave for peak, N and P waves). Recording VECAPs requires special techniques to reduce or even eliminate stimulation artifact which is generated due to proximity of stimulation and recording electrodes.

VECAPs occur within the first millisecond after onset of electrical stimulation. This is significantly faster than a VOR response and would be apt for a closed-loop VI. In Part II we demonstrate acquisition of VECAPs and correlation with VOR responses in guinea pigs.

Restoration of vestibular function We have discussed vestibular neurophysiology and the components of a VI. Figure 2.2E shows the experimental chain for the horizontal canal in a rhesus monkey (Dai et al., 2011). First, the subject experienced whole body rotation around its lateral axis. VOR responses in this normal condition were predominantly horizontal. Second, sequential gentamicin treatment of the ears eliminated vestibular function. Third, with an activated VI, eye movement could be partially restored. However, there was asymmetry, i. e. the response was stronger in one head direction than the other, mimicking a unilateral vestibular impairment. Additionally, VOR responses along the undesired axes LARP and RALP were observed.

This illustrates remaining challenges in VI development: subpar VOR responses, misalignment (erroneous eye movement along non-desired axes) and asymmetry. Next, Part I investigates which stimulation paradigm evokes VOR responses more effectively during acute stimulation in patients. Part II characterizes VECAPs in relation with VOR in guinea pigs that may lead to a closed-loop VI and to overall better implant performance. Part III summarizes findings and highlights remaining issues that need to be addressed in future VI development.

Part I

ASSESSING PULSE AMPLITUDE AND PULSE RATE MODULATION IN INSTRUMENTED BVL PATIENTS

REAL-TIME RESEARCH PLATFORM FOR HUMAN VESTIBULAR IMPLANTS

Abstract Researchers have succeeded in partly restoring damaged vestibular functionality in several animal models. Also acute interventions have been demonstrated in human patients. Our previous work on a vestibular implant for humans used predefined stimulation patterns that could not be modulated by an external sensor. Here we present a research tool that facilitates motion-modulated stimulation. This requires a system that can process gyroscope measurements and send stimulation parameters to a hybrid cochlear-vestibular implant in real-time. To match natural vestibular latencies, the time from sensor input to stimulation output should not exceed 10 ms. We describe a system based on National Instrument's CompactRIO platform that can meet this requirement and also offers floating point precision for advanced transfer functions. It is designed for acute clinical interventions, and is sufficiently powerful and flexible to serve as a development platform for evaluating prosthetic control strategies. Pulse amplitude and pulse rate modulation to predetermined functions or sensor inputs have been validated. The system has been connected to human patients, who each have received a modified MED-EL cochlear implant for vestibular stimulation.

This chapter has been published almost as is in: Nguyen TAK, Ranieri M, DiGiovanna J, Peter O, Genovese V, Perez Fornos A, and Micera S. A Real-Time Research Platform to Study Vestibular Implants With Gyroscopic Inputs in Vestibular Deficient Subjects. Biomedical Circuits and Systems, IEEE Transactions on 8: 474-484, 2014.

3.1 INTRODUCTION

Preliminary vestibular implant trials in human subjects returned promising results (Guyot et al., 2011ab). Our collaborators performed that study with one bilaterally deaf patient who furthermore suffered from bilateral vestibular loss. He received a unilateral, modified cochlear implant with one electrode of the cochlear electrode array placed close to the posterior ampullary nerve. Once adapted to baseline stimulation, sinusoidally modulated pulse amplitude or pulse rate of the stimulation signal successfully generated smooth sinusoidal eye movements.

To extend that study and move towards a vestibular implant in humans, the next logical step is to drive the modulation with a motion sensor (e.g., gyroscope) attached to the patient's head. The objective is to measure the subject's head rotation and to mimic the natural function of the semicircular canals. This requires the development of a technical system with low latency and jitter able to process incoming rotational signals and to communicate with the implanted cochlear-vestibular implant. Healthy VOR response times in humans – from head movement change to eye movement onset – were reported between 7.5 to 10.3 ms with standard deviations of 2-3 ms (Aw et al., 1996). Therefore to scale with these normal response times, the response time of the system from sensor input to stimulation output should not exceed 6.5 ms as the delay from pulse train stimulation to eye movement is approximately 3.5 ms (Cohen et al., 1963).

The system presented herein is intended as research platform to help define design constraints for an eventually wearable vestibular implant in humans. (As is, it is only suitable for acute clinical therapies.) Pulse amplitude modulation, pulse rate modulation, and a combination of both are required, since it remains open to debate which paradigm is most effective and efficient in humans. The vestibular system intrinsically works with spike rate modulation, rendering pulse rate modulation the apparent choice for encoding angular velocity and has been tested successfully in animal models. On the other hand, pulse amplitude modulation has yielded excellent results in other sensory neuroprostheses, such as cochlear implants. Also a combination of both modulation paradigms in animal models has demonstrated efficacy evoking larger eye movement responses than the individual modulation modes (Davidovics et al., 2012, 2013). Thus, this platform was designed to accommodate all three modulations modes.

Other design considerations were extensibility and usability. It was necessary to be able to add more advanced mapping functions later, and the user interfaces needed to be well-arranged and easy to use in acute clinical tests. The selected system has floating point capabilities allowing for more elaborate mapping functions, and the accompanying LabVIEW software facilitates a quick setup of flexible user interfaces.

The next sections detail the system's hardware components, software architecture and operating modes. Validation results from bench tests are discussed, too.

3.2 SYSTEM ARCHITECTURE

In our clinical trials a modified PULSAR cochlear implant (Med-El, Innsbruck, Austria) stimulates the semicircular canals. Up to three electrodes can be designated for vestibular stimulation, i.e. one per canal. To communicate with the implant, our system uses a digital protocol and is connected to a customized Direct Research Interface Box (dRIB). The hardware system features three levels to achieve the low response time and to implement the digital protocol (Fig. 3.1):

1. Field Programmable Gate Array (FPGA) for communication with the dRIB,
2. Real-Time (RT) controller for processing gyroscope readings and compute corresponding stimulation parameters, and
3. PC for programming and setting parameters, as well as monitoring sensor input and stimulation outputs.

In the general operating scenario, the operator specifies stimulation strategy and monitors angular velocities and stimulation parameters on a PC screen. After setting basic parameters (e.g., baseline pulse rate and amplitude), the stimulation is activated and the stimulation signal is increased to baseline level. Then the operator can activate amplitude or pulse frequency modulation to gyroscope readings or to a defined sinusoidal function. Pulse parameters are continuously sent from the FPGA to the dRIB interface box that transmits an encoded data stream through a transmission coil to the cochlear implant, where the stream is converted into corresponding stimulation pulses.

3.2.1 *Hardware*

Gyroscope A wearable unit containing a MEMS gyroscope has been developed for the experiments with implanted patients (Carpaneto et al., 2015). The sensor was a 3-axis gyroscope (LYPR540AH by ST Microelectronics, Geneva, Switzerland) capable of measuring yaw, pitch and roll.

Anti-aliasing filters were added, and the PCB with all components was encased in a 44x75x11 mm metal box. A titanium screw on one side of the box allows for transcutaneous fixation to a subject's mastoid. A 2 m long cable carries the three angular rates, and two other lines for DC power supply (two AA batteries for safety reasons).

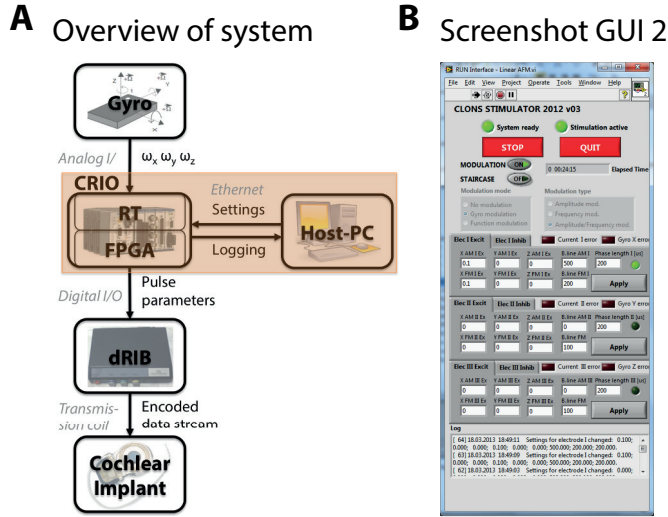


Figure 3.1: System overview and user interface. (A) From top: A gyroscope senses rotation and is connected to the analog input interface of the CompactRIO (CRIO). It features a real-time (RT) controller and a field programmable gate array (FPGA). The RT controller exchanges data with a host-PC via ethernet. RT, FPGA and PC (orange block) constitute the core of the system. Parameters are sent digitally from the FPGA to the direct Research Interface Box (dRIB) that translates them into MED-EL's proprietary data stream. The stream is sent through a transmission coil to the cochlear-vestibular implant that generates the appropriate stimulation pulses. (B) The main interface (GUI 2) during stimulation. The operator starts and stops the stimulation, selects modulation mode and type (PAM, PRM, PAM/PRM), and specifies gains and baselines for the three controlled electrode sites. A log at the bottom displays the events.

CompactRIO (CRIo) We opted for National Instruments' CRIo platform (NI, Austin, TX, USA) as research tool for several reasons: (i) powerful embedded controller; (ii) integrated FPGA for digital communication; (iii) LabVIEW's ease to program GUIs; and (iv) compliance with safety standards and directives (IEC 61010, IEC 60601-1).

Specifically, we assembled a system with the NI cRIO-9113 chassis (Virtex 5 FPGA), CRIo-9022 embedded controller, one NI 9205 analog input module, three NI 9401 digital input/output modules, and the power supply module NI-PS 15. The Virtex-5 LX50 FPGA had 48 multipliers and 28'800 flip-flops, the embedded controller a 533 MHz CPU, 2 GB solid-state storage and 256 MB DRAM. Both CPU and FPGA were mid-range performance components recommended by NI for our scenario. The analog input module NI 9205 with 250'000 samples per second was sufficiently fast for three input channels (sampling period of up to 12 µs). The digital module NI 9401 had a fast update rate of 100 ns to facilitate the communication between the FPGA and dRIB. A 34-pin flat ribbon cable for 16 data, three address, one enable, and ready bits connected the three modules with the dRIB. Data was transmitted when ready was set low by the dRIB; then the CRIo pulled the enable signal low for at least 300 ns. The whole system weighed 2.3 kg.

Direct Research Interface Box (dRIB) Generally, Med-El implants convert a digitally encoded data stream to stimulation pulses. The format of this data stream is proprietary. Therefore, a device was needed to translate pulse properties — such as pulse amplitude, phase duration, controlled electrode site — into that stream with low latency. Current research tools for Med-El implants could not be used due to load-dependent response times of about 200 ms with large jitter (unpublished). We built the dRIB on the basis of a previous device for Med-El implants (RIB1) that contained a microprocessor and a FPGA section for data encoding (Baumann and Nobbe 2006). Disabling the internal microprocessor allowed for an external 16-bit input that would send stimulation parameters from the CRIo. Additionally, a level shifter and boot-time disconnection logic were built and added to translate between the different logic levels of the CRIo and the dRIB. The dRIB provided lowest possible latencies: from completely written pulse data to pulse output $21 \times 1.67 \mu\text{s} = 35 \mu\text{s}$ (16 data bits, 3 address and 2 read/write bits at a transfer rate of 600 kHz from dRIB to implant). The interface box also guaranteed that only valid data was transmitted and ensured continuous power supply for the implant without specific knowledge of the data format.

Personal computer (PC) All PCs used to program the Crio ran Windows 7 (Microsoft Corporation, Redmond, WA, USA) and had LabVIEW 2011 with the RT and FPGA modules installed (National Instruments). PC CPU speed was not critical for performance. A LAN port was required to connect to the Crio.

3.2.2 Software

Four different GUIs were implemented in LabVIEW: (i) a GUI with controls for configuration and monitoring; (ii) a GUI with stimulation settings; (iii) a GUI for RT processing and (iv) a GUI to monitor outgoing communication from the FPGA.

These GUIs are specifically designed for the different hardware levels. GUIs 1 and 2 are executed on the PC, GUI 3 on the RT controller and GUI 4 on the FPGA. Figure 3.2 shows the interconnection of the Crio components and the GUIs, Fig. 3.3 illustrates the flow charts of GUIs 3 and 4.

GUI 1: controls for configuration and monitoring This GUI has five tabs and is the main interface before start of stimulation. The first tab includes charts of angular velocities, pulse rates and pulse amplitudes. The second tab loads gyroscope calibration values and sets a phase delay (to delay acting on processed gyro input values, e.g. to mimic the time constant of the semicircular canals). Calibration values map the gyroscope coordinate system to the patient's reference frame (DiGiovanna et al., 2012). The third tab specifies controlled electrode sites, current ranges (four ranges with 128 steps: 150, 300, 600, 1200 current units, 1 cu equals approximately 1 μ A and implant types (PULSAR/SONATA implant for clinical trials and benchmark tests or C40+ implant for benchmark tests only). The operator chooses a location where to save log files with the fourth tab. The final tab sets sinusoidal modulation of pulse amplitude and pulse rate.

GUI 2: stimulation settings This GUI is most relevant for the operator during stimulation and its design was shaped by feedback from two clinicians and two engineers (Fig. 3.1B). It features START/PAUSE and QUIT buttons. The operator selects between modes 'No modulation', 'Gyro modulation', or 'Function modulation', and between types 'Amplitude modulation' (PAM), 'Rate modulation' (PRM), or 'Amplitude/Rate modulation' (PAM/PRM). Two other controls toggle modulation and the staircase function (described further below).

Three panels set gains, phase length (length of cathodic and anodic phase, respectively), baseline pulse amplitude and pulse rate for each of the three electrode sites. Depending on the operating type, non-relevant control parameters are disabled. Furthermore, the operator is able to choose between symmetric or non-symmetric stimulation. Choosing the former, gains were identical for positive and negative angular velocities; choosing the latter allowed the operator to specify another set of gain values for negative angular velocities, effectively resulting in a piecewise linear transfer function. More advanced functions may be loaded in future software versions.

A log displays events such as start of stimulation and warnings. Each entry triggered a digital output for synchronization with video recordings and post-hoc analysis.

GUI 3: real-time controller This GUI is deployed to Crio's embedded controller and has an empty graphical interface, since any interactive item would affect RT performance. The algorithm has two parts: a time-critical loop with high priority and a non-critical loop with lower priority. The non-critical loop runs every 200 ms and is responsible for data exchange between both GUIs 1 and 2 (on PC) and the GUI 3 on the embedded controller. Specifically, undeterministic network variables are copied to deterministic RT equivalents for use in the time-critical loop. The loop time of 200 ms was chosen to transfer stimulation parameters to the PC for logging as often as possible but without over-burdening the embedded controller with variable conversion.

The time-critical loop processes incoming gyroscope voltages and calculates stimulation parameters; it runs every 2 ms. The conversion from voltages to angular velocities involves a 3x3 matrix multiplication with the three voltages. Pulse amplitude and pulse rate are calculated according to Eqs. (3.1)-(3.4) depending on operating mode and type. Pulse parameters are then sent to GUI 4. In principle this loop should run as often as possible. However, the execution time was 1.2 ms; thus the loop time had to be set to the next full millisecond (2 ms) to comply with LabVIEW's Timed Loops.

GUI 4: FPGA This GUI is responsible for input and output communication. Upon start it initializes the dRIB. Then it periodically acquires and buffers gyro voltages (16-bit ADC) every millisecond. Each electrode site has a loop that writes stimulation parameters into a FIFO buffer at the time point specified by the pulse frequencies. For instance at 100 pulses per second (pps), the loop executes every 10 ms and writes the parameters for one stimulation pulse into the FIFO.

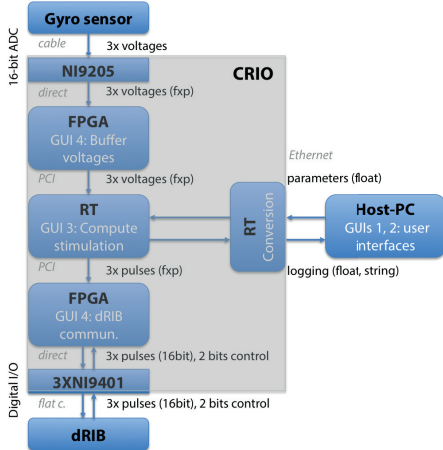


Figure 3.2: Interconnections and signal flow between components. From top: Analog voltages for yaw, pitch and roll are digitized (NI9205) and buffered with GUI 4 on the FPGA as fixed point variables (fpx). Via the PCI bus, the values are read from GUI 3 running on the RT controller to compute current amplitude and pulse rate (floating point). Parameters are sent through Ethernet from the host PC (GUIS 1, 2) and have to be converted to deterministic RT variables. Stimulation values are then transmitted in GUI 4 through the three NI 9401. A flat ribbon cable that has 16 data, 3 address and two control bits (enable, ready) connects the digital modules with the dRIB.

Due to the structure of these write loops, a special mechanism is implemented for low pulse frequencies less than 40 pps. For example with 10 pps, the loop would run only every 100 ms and write a pulse to the FIFO buffer. With PAM this does not pose a problem. However with PRM, this would prevent swift changes of pulse rates. Therefore, the mechanism checks every 25 ms whether the pulse rate has increased beyond 40 pps and replaces the old stimulation pulse parameters with new ones if necessary. This gives priority to pulses with higher pulse rate. The 40 pps threshold was an educated guess, and can be tuned by the operator.

Another part of the FPGA code checks the FIFOs every 0.5 ms and arbitrates in case pulses are scheduled simultaneously. Priority is given to the pulse with the highest pulse rate. If pulses have identical rates, output on electrode I comes before electrode II that comes before electrode III. The dRIB and the cochlear implant are not capable of activating electrode sites simultaneously (instead the next site would be activated 0.5 ms later). GUI 4 is usually hidden and provides operators with advanced options such as overriding input signals.

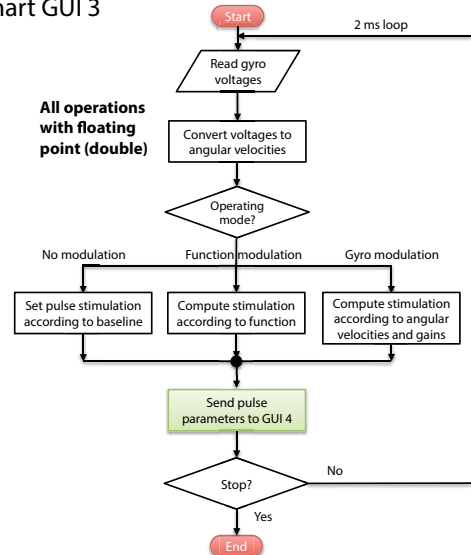
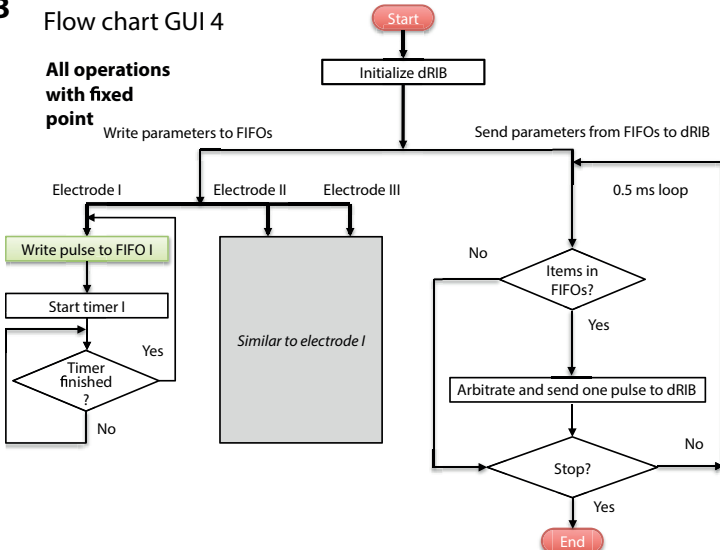
A Flow chart GUI 3**B** Flow chart GUI 4

Figure 3.3: Flow charts of GUIs 3 and 4. All operations in GUI 3 are done with floating point, in GUI 4 with fixed point. (A) The time-critical loop of GUI 3 starts with reading gyroscope voltages and converts them to angular velocities. Pulse parameters are then computed depending on the operating mode and sent to GUI 4 (green shaded box). The distinction between PAM, PRM and PAM/PRM is done inside the computation boxes and was excluded here for legibility. Commands are repeated every 2 ms. (B) GUI 4 for the FPGA runs code extensively in parallel. After initialization of the dRIB, pulse parameters – received from GUI 3 (green shaded box) – are written into FIFOs for each electrode. Timers are run to create a certain pulse rate (e.g., a timer of 10 ms for 100 pps). Simultaneously, another loop checks every 0.5 ms whether the FIFOs are filled and sends out existing pulses to the dRIB giving priority to the pulse with the highest pulse rate.

3.2.3 Implementation of operating modes and types

This section elaborates on the various modulation modes. It also explains the inherent difficulty of implementing PRM using current cochlear implant technology. All gain and baseline parameters are taken from the GUIs 1 and 2.

Mode ‘No modulation’ This mode provides steady-state stimulation at the specified baseline pulse amplitudes and baseline pulse rates. In PAM mode, baseline pulse rates are identical for all three electrodes, and different baseline pulse amplitudes can be set. In PRM or PAM/PRM mode, each electrode has its own set of baseline values for both pulse amplitude and pulse rate.

In this mode the staircase function is activated per default. It adapts subjects slowly to baseline stimulation as a sudden change in stimulation amplitude would be perceived as an abrupt change in head rotation and may result in severe symptoms such as nystagmus, vertigo and nausea. It increases current amplitude by 50 cu every 100 ms, while pulse rate remains constant at baseline level. Vice versa, when stimulation is turned off, pulse amplitude is decreased by the same ratio.

Mode ‘Function modulation’ This mode modulates pulse amplitude and/or pulse rate according to a sinusoidal function regardless of gyro inputs (i.e., no patient movement required). Theoretically, modulation frequencies of up to 500 Hz are possible, but frequencies up to 8 Hz are physiologically most relevant (Pozzo et al., 1990). In PAM mode, the current amplitude is calculated as:

$$I_1 = R_A \sin(2\pi ft) + b_{A_1} \quad (3.1)$$

where R_A is the modulation range (identical for all electrode sites), f the modulation frequency, t the elapsed time since the start of function modulation, and b_A the baseline pulse amplitude.

In PRM mode, the pulse frequency is determined as:

$$P_1 = R_P \sin(2\pi ft) + b_{P_1} \quad (3.2)$$

where R_P is the modulation range for the pulse rate, and b_P the baseline pulse rate. Selecting the mixed mode PAM/PRM combines Eqs. (3.1) and (3.2).

Mode ‘Gyro modulation’ This mode modulates parameters depending on the baseline values, gains and measured angular velocities, i.e. it mimics the rotation-based modulation of the vestibular system.

With PAM, stimulation pulses have a fixed pulse rate and pulse amplitude is computed as:

$$I_1 = g_{A_{x_1}} \omega_x + g_{A_{y_1}} \omega_y + g_{A_{z_1}} \omega_z + b_{A_1} \quad (3.3)$$

where I is the current amplitude, b_A the baseline amplitude, and g_A the PAM gains for the three angular velocities ω_x , ω_y and ω_z . The suffix 1 indicates electrode site 1. Equations for sites 2 and 3 are similar, but with different gains and baseline values. The current amplitude I and baseline amplitude b_A had the unit [cu], the gains [cu/(°/s)], and angular velocities [°/s]. If non-symmetric stimulation is chosen, then gains have different values for non-negative and negative angular velocities.

With PRM, the pulse amplitude is fixed to the baseline pulse amplitude and pulse rates are modulated as:

$$P_1 = g_{P_{x_1}} \omega_x + g_{P_{y_1}} \omega_y + g_{P_{z_1}} \omega_z + b_{P_1} \quad (3.4)$$

where P is the pulse rate, b_P the baseline pulse rate, and g_P the PRM gains. Similar equations are in place for electrode sites 2 and 3. Again, a second set of gains can be specified for negative angular velocities. The units were [pps] for P and b_P and [pps/(°/s)] for the gains. The mixed mode PAM/PRM combines Eqs. (3.3) and (3.4): modulating both pulse amplitude and pulse rate, which can be regarded as the superposition of the two individual modes.

Remarks on pulse rate modulation with cochlear implants Cochlear implants employ PAM as primary means to provide cues for speech recognition. Therefore, it can be directly implemented via interfacing with the dRIB registers for stimulation amplitude. However, there is no dRIB register to specifically set the pulse rate of each electrode site separately. Instead stimulation pulses are sent from CRI to dRIB at appropriate fixed intervals to render baseline pulse rate.

Due to the lack of a pulse rate generator in the dRIB, PRM can only be emulated on the CRI with the limitations explained below. Given the code structure of GUI 4, pulses are transmitted at most every 0.5 ms, resulting in intervals of 2, 2.5, 3 ms etc. (minimum interval of 2 ms) equivalent to pulse frequencies of 500, 400, 333 pps etc. Values like 450 pps are achieved by switching between 500 and 400 pps (i.e., pulse rate averaging). This creates a non-linear resolution of pulse rates with higher accuracy for lower pulse rates. This resolution is the most acceptable, given typical stimulation parameters. We decided to avoid shorter intervals, such as 0.2 ms, as they could result in a loss of pulses.

3.2.4 Validation

Methods The following features were tested:

1. Response time (sensor input to stimulation output)
2. Mode: function modulation
3. Mode: gyro modulation
4. Phase delay

To visualize stimulation pulses, a detector box acted as a substitute for a cochlear implant. A transmission coil from the dRIB was connected to a C40+ detector box for PAM and for PRM tests (Department of Ion Physics and Applied Physics at the University of Innsbruck, Innsbruck, Austria). It simulates a patient's implant impedances with one resistor per electrode site. The PAM/PRM mode was validated with a PULSAR detector box (also University of Innsbruck). The two types of detector boxes differ slightly, the C40+ has a more non-linear current output (in amplitude). Both boxes had to be tested, since either could be used in clinical trials to monitor the output to the patient. In benchmark tests, stimulation pulses were recorded with a Tektronix MSO2014 (Tektronix, Beaverton, OR, USA) and Tektronix' modified version of LabVIEW Signal Express 2011.

The response time was measured with voltage step inputs from 0.9 to 2.3 V, representing a change of angular velocity from -700 to 950 °/s. The steps were applied with frequencies from 0.25 to 20 Hz to cover a wide range of possible motion changes. (Frequencies of head movement in various locomotor tasks had harmonics up to 8 Hz or 20 Hz (Grossmann et al., 1988).) The step input was applied to one input channel, the other two channels were kept at 0 V. Test inputs were generated with a TTi TG330 function generator (Thurlby Thandar Instruments, Huntingdon, UK).

Function modulation was tested in AM and FM modes for different modulation frequencies. The tested range of 200 ± 150 pps was typical for vestibular prosthesis prototypes (Merfeld et al., 2007). The PAM/PRM mode was validated in a single test covering the appropriate ranges in both modulation domains.

Sinusoidal voltage inputs for gyro modulation were generated with the TTi function generator. Additionally, a programmable phase delay was tested at 50 ms. All test parameters are listed in Table 3.1.

Table 3.1: Settings for Crio validation

Function mod.	Baseline pulse amplitude [cu]	Baseline pulse rate [pps]	Range	Mod. freq. [Hz]	
PAM	500	500	400 cu	2; 5	
PRM	500	200	300 pps	2; 5	
PAM/PRM	300	200	400 cu 300 pps	2	
Gyro mod.	Baseline amplitude [cu]	Baseline pulse rate [pps]	Gain	Phase delay [ms]	Input freq. [Hz]
PAM	500	500	0.1 cu/(°/s)	0	2; 5
PAM	500	500	0.1 cu/(°/s)	50	2
PRM	500	500	0.1 cu/(°/s)	0	2; 5
PRM	500	500	0.1 cu/(°/s)	50	2

Note: 500 pps represents a worst-case load; 200 pps represents a reasonable baseline pulse rate. We could not test worst-case in PRM as it would not have been possible to up-modulate.

Analysis To assess performance we calculated latencies between the ideal output (reference signal) and the measured output. Root Mean Square Errors were computed with consideration of quantization errors (RMSE_{QE}). These are presented in the sections below. For reference we also report the RMSE_{ZQE} assuming a zero quantization error, i.e., an ideal output device. All analysis was done in Matlab 2011a (MathWorks, Natick, MA, USA).

3.3 RESULTS

3.3.1 Response time

Figure 3.4 shows response times at 200 and 500 pps to a voltage step from 0.9 to 2.3 V (equivalent to -700 to 950 °/s). The step had a frequency of 5 Hz; the system was in gyro modulation mode PAM. One hundred measurements were taken. At 200 pps, response times for rising and falling edges averaged at 6.8 ms, standard deviation was 1.6 ms, and the maximum latency was 9.95 ms. At 500 pps, values were 5.2, 0.8, and 6.6 ms, respectively. The lower variance for the higher pulse frequency was also reflected in the histogram, where 40% of samples were between 4.5 and 5.5 ms in contrast to 16% for 200 pps. Other step frequencies between 0.25 and 20 Hz did not significantly change results.

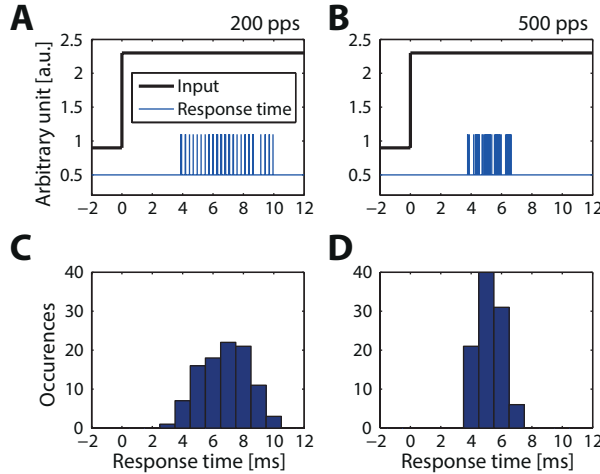


Figure 3.4: Response time. (A) At 200 pps, the system responded to a step input (black trace) with a range of latencies from 4 to 10 ms. (B) At 500 pps, the range is smaller from 4 to 6.5 ms, showing that response time was affected by baseline pulse rate. (C) and (D) show the histograms of response time for the two different conditions (total occurrences 100 each). At 200 pps, response times were more widely distributed. In contrast, at 500 pps, 40% of response times were within 4.5 and 5.5 ms.

Mode ‘Function modulation’ Pulse amplitude and/or rate were modulated as described in Eqs. (3.1) and (3.1). Figure 3.5 shows function modulation for 2 and 5 Hz modulation frequencies. PAM function modulation demonstrated only small lags (2.3 and 0.4 ms positive peak lag and 1.7 and 0.1 ms negative peak lag). RMSE_{QE} was zero (considering the quantization error of ± 13.4 cu, i. e. the implant has limited pulse amplitude resolution), see Table 3.2.

In PRM mode, modulation range was 150 pps at a baseline pulse rate of 200 pps. Pulse rate steps were starkly noticeable at low frequencies. At high pulse frequencies, pulse rates had higher variance. The positive peak lags were 4.0 and 1.5 ms for 2 and 5 Hz; the negative peak lags 7 and -4.5 ms, respectively. RMSE_{QE} were less than 5 pps (2.5% of baseline).

Figure 3.5E, F depicts PAM/PRM at 2 Hz modulation frequency. In contrast to the other plots, parameters were slightly different and these traces were not averaged since only a single 2 second trial was included. The lags were small: 3.5 ms for the positive peak and 0.0 ms for the negative peak (PAM), -16.5 ms and 0.0 ms for PRM. RMSE_{QE} values were 0 cu and 9.2 pps (0 and 4.6% of baseline, respectively).

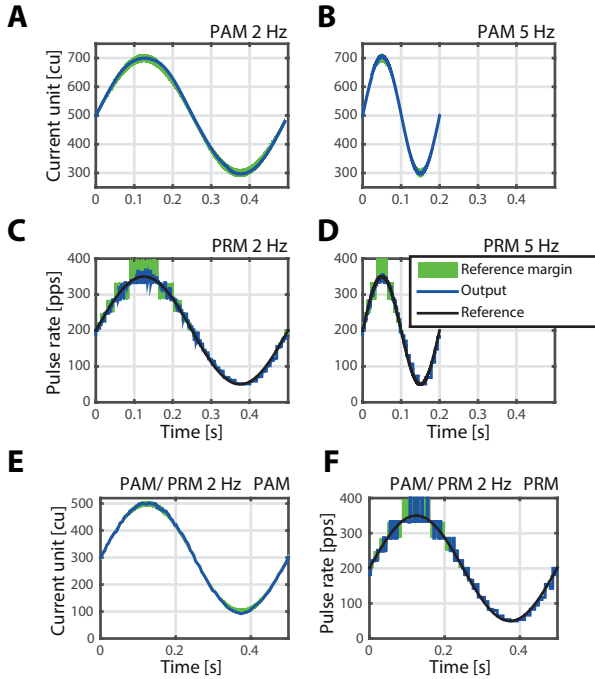


Figure 3.5: Validation of function modulation. (A) Modulation of pulse amplitude at 2 Hz and 200 cu magnitude at 500 cu baseline. (B) Modulation at 5 Hz. In both cases, the averaged measured output (blue) agreed with the reference (green band) showing RMSE_{QE} of zero (accounting for quantization error). (C) and (D) show modulation of pulse rate at 2 and 5 Hz. The black lines in PRM plots illustrate the exact reference, while the green band illustrates the margin of error due to the non-linear pulse rate resolution. RMSE_{QE} was 1.4 pps for 2 Hz and 3.4 pps for 5 Hz. At low pulse rates the limited resolution became clearly visible. (E) and (F) represent a single trial (not averaged) of the combined PAM/PRM mode. The trial lasted 2 seconds, and the plots show the first 0.5 s to match subplots A-D. RMSE_{QE} were 0 cu and 9.2 pps. All lags are summarized in Table 3.2.

Table 3.2: Statistics for CRI0 function modulation

Test	Lag pos. peak [ms]	Lag neg. peak [ms]	RMSE _{QE}	RMSE _{ZQE}
PAM 2 Hz	2.3	1.7	0 cu (0%)	5.1 cu (1.0%)
PAM 5 Hz	0.4	0.1	0 cu (0%)	4.1 cu (0.8%)
PRM 2 Hz	4.0	7	1.4 pps (0.7%)	8.8 pps (4.4%)
PRM 5 Hz	1.5	-4.5	3.9 pps (2%)	10.7 pps (5.4%)
PAM/PRM: PAM	3.5	0.0	0 cu (0%)	4.2 cu (1.4%)
PAM/PRM: PRM	-16.5	0.0	9.2 pps (4.6%)	15.4 pps (7.7%)

Lags and RMSE for individual PAM and PRM tests were calculated from averages, whereas the values for the combined PAM/PRM test were taken from a 2 second single trial. Two RMSE values were computed to account for the quantization error RMSE_{QE} and to compare it to an ideal output with zero quantization error RMSE_{ZQE}, i.e. the reference signal had zero tolerance. RMSE values in brackets are in percent of baseline.

Table 3.3: Statistics for CRI0 gyroscope modulation

Test	Lag pos. peak [ms]	Lag neg. peak [ms]	RMSE _{QE}	RMSE _{ZQE}
PAM 2 Hz, 0 ms	5.5	1.4	0 cu (0%)	5.8 cu (1.2%)
PAM 2 Hz, 50 ms	4.2	0	0 cu (0%)	6.9 cu (1.4%)
PAM 5 Hz, 0 ms	2	2.4	0 cu (0%)	5.3 cu (1.1%)
PRM 2 Hz, 0 ms	6.2	13.9	7.9 pps (4%)	12.3 cu (6.2%)
PRM 2 Hz, 50 ms	10.8	12.9	7.9 pps (4%)	12.3 cu (6.2%)
PRM 5 Hz, 0 ms	5.5	11.8	20.8 pps (10.4%)	27.6 cu (13.8%)

Mode ‘Gyro modulation’ The main objective of the new system was to couple modulation of the stimulation signal to a 3-axis gyroscope sensor in real-time (we had tested function modulation in humans before). Validation results are depicted in Fig. 3.6. The top row shows PAM, the bottom row PRM for one output channel. Tests not reported herein with all input and output channels active showed correspondingly similar results.

Due to the function generator’s DC settings, the input was slightly unsymmetrical peaking at -750 and +1000 °/s. Measurements were averaged over 50 samples for 2 Hz and 100 for 5 Hz. A reference signal was calculated from the input signal ω_x , and a gain of 0.1 cu/(°/s) for $g_{A_{x_1}}$ PAM or 0.1 pps/(°/s) for $g_{P_{x_1}}$ PRM (cf. Eqs. (3.3)-(3.4)). All other gains were zero. The graphs in the left and right columns had no phase delay, the center column had a 50 ms phase delay.

In PAM, the measured output followed the reference. Differences were less than the quantization error. The positive peaks of input and output lagged 5.5 ms for 2 Hz sinusoidal input and 0 ms delay, 4.2 ms for 50 ms phase delay, and 2 ms for 5 Hz and 0 ms delay. The lags for the negative peak were 1.4, 0.06, and 2.4 ms, respectively. These statistics and $RMSE_{QE}$ equaling zero are summarized in Table 3.3.

In PRM, the baseline pulse rate was 200 pps. Two main observations were made. First, a high variance of pulse rate was recorded for pulse rates above 250 pps. Second, the output lagged the reference more for negative than positive angular velocities (13.9 vs 6.9 ms for 2 Hz, 0 ms delay). The latencies for other scenarios did not exceed 13 ms and are shown in Table 3.3. $RMSE_{QE}$ was about 7.9 pps for both 2 Hz cases and 20.8 pps for 5 Hz stimulation (4 and 10.4% of baseline pulse rate, respectively).

3.4 DISCUSSION

Our system’s primary design constraint was that the latency between acquiring angular velocities and modulating stimulation output should not exceed 6.5 ms. The performance of our system remained below or close to the limit; all modulation modes were accurate. These diverse modes have previously shown effects on eye movement responses in animal models (Davidovics et al., 2012, 2013). With our system we will be able to evaluate which paradigm is optimal in humans; this insight will be critical for design of future portable vestibular prosthetics.

System architecture Vestibular prostheses for animal models have employed tailored circuits typically with microcontrollers (Gong and Merfeld, 2000;

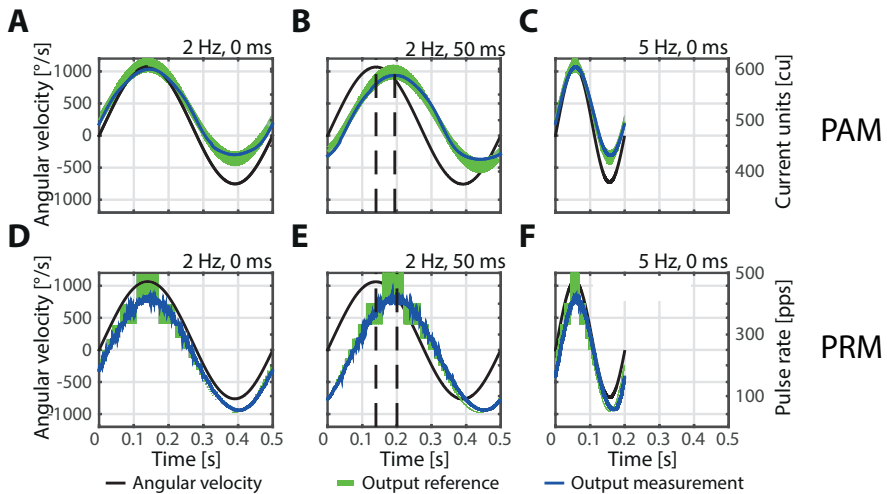


Figure 3.6: Validation of gyro modulation. PAM (A-C) and PRM (D-F). (A) Baseline pulse amplitude was 500 cu and baseline pulse rate 500 pps. The black trace illustrates averaged input angular velocity, the green band the desired output signal and blue trace the averaged output. The input signal had a frequency of 2 Hz and no input delay. RMSE_{QE} was 0 cu. (B) Same as (A) but with an input delay of 50 ms (vertical dashed lines). Reference and measured output shifted accordingly and RMSE_{QE} was 0 cu. (C) A higher input frequency of 5 Hz did not affect the output signal and remained within the reference. (D) Baseline pulse rate was 200 pps. The averaged measured output followed the reference, but showed large variance at high pulse rates and a visible lag at low pulse rates. The lag for the positive peak was 6.2 ms, for the negative peak 13.2 ms. RMSE_{QE} was 7.9 pps (4% of baseline rate). (E) Same as (D) but with 50 ms input delay depicted by the two black dashed lines. Output was also delayed by 50 ms. RMSE_{QE} was very similar to (D). (F) At a higher input frequency of 5 Hz, RMSE_{QE} increased to 20.8 pps, while lags were comparable to (D) and (E).

Fridman and Della Santina, 2012), or alternatively with CMOS technology (Constandinou et al., 2008), or with a field-programmable analog array (Toreyin and Bhatti 2013). These low-cost systems can provide faster response times, but translation to clinical studies in patients has remained difficult. The use of modified, commercially available, cochlear implants offers a fast-track to a vestibular implants in humans since it is based on established and medically certified technology. Our system with a modified implant is not portable, but is intended as research platform and provides clinicians with flexibility to study stimulation paradigms and parameters. Additionally, some restrictions applied due to interfacing the proprietary implant software (forced through the dRIB). These aspects should be regarded as confounds when comparing the CRIo system with others.

Two groups have tested modified cochlear implants in rhesus monkeys: one based on a Concerto MED-EL implant (Valentin et al., 2013), the other one on Nucleus Freedom implant (Cochlear Corporation) (Phillips et al., 2011; Nie et al., 2013). The former had a belt-worn unit with a Bluetooth interface to tune parameters and a head-worn unit with a gyroscope and radio frequency link to the implanted stimulator. The system was portable. Similar to our approach, their software used a ‘time-until-next-pulse’ to create pulse rate stimulation. For the modulation, parameters were determined with a 32 bin look-up table (Valentin et al., 2013), whereas our system performed floating point calculation. Regarding the other implant, a setup with a research processor applied various pulse trains (similar to our function modulation) (Nie et al., 2013); for real-time processing (gyro modulation) one had to switch to another setup with a clinical processor (Phillips et al., 2011). The CRIo can transition between function and gyro modulation seamlessly.

These other systems delivered in-vivo results consistent with earlier work of those groups. However, they did not report response times, or elaborate on implementing pulse rate modulation with cochlear implant technology.

Response time At 200 pps baseline pulse rate, our average response time from sensor input to stimulation output was 6.8 ms with a standard deviation of 1.6 ms. At 500 pps, the values were 5.2 and 0.8 ms. Latencies from pulse train stimulation to eye movement in cats were measured at 3.8 ms (200 pps) or 3.5 ms (500 pps) (Cohen and Suzuki 1969). Latencies to single pulses were timed at 5-6 ms in cats (Cohen and Suzuki 1969) or squirrel monkeys (Merfeld et al., 2007). Therefore, the total response time from sensor input to eye movement onset with our system can be stated as 10.6 ± 1.6 ms for 200 pps or 8.7 ± 0.8 ms for 500 pps. These would be within the range of natural response

times (7.5 ± 2.9 , 7.6 ± 2.8 , and 10.3 ± 1.9 ms for yaw, pitch and roll, respectively (Aw et al., 1996)). Though our system would be slightly slower for two axes, the VOR has demonstrated high adaptability. For instance, VOR gains and phase as well as alignment improved with chronic stimulation (Lewis et al., 2002; Dai et al., 2011). These findings suggest that the VOR response could adapt to the suboptimal CRIo stimulation. Additionally, the impact of a slower response time could be studied with the ‘phase lag’ parameter.

The maximum CRIo latency observed at 200 pps was 9.95 ms. Theoretically, the maximum response time was 10.5 ms, composed of 4 ms to read and process an input change, 3×0.5 ms to send pulse parameters for three electrodes and 5 ms for the pulse period at 200 pps ($4\text{ ms} + 3 \times 0.5\text{ ms} + 1/200\text{ pps}$). Reading and processing were performed in GUI 3, the output of pulse parameters in GUI 4. Likewise at 500 pps, we observed a maximum latency of 6.62 ms, the highest theoretical value was 7.5 ms. The response time could be reduced by activating only one electrode site and thus lowering the number of calculations and writing operations. This could halve the processing time (time-critical loop of GUI 3) and the maximum time from input to stimulation output at 200 pps would be 4.5 ms ($2\text{ ms} + 1 \times 0.5\text{ ms} + 1/200\text{ pps}$). A similar improvement could be achieved with a stronger processor than 533 MHz. These improvements will be implemented if clinical tests prove them to be necessary.

Pulse rate influenced latencies. The higher the pulse rate, the sooner an updated pulse could be applied. The 200 pps baseline pulse rate, that was tested agrees with the common approach in unilateral implants to use a higher than normal baseline pulse rate to evoke both excitatory and inhibitory eye movement responses. Human subjects have been adapted to baseline pulse frequencies of 200 pps (Guyot et al., 2011a) and 400 pps (unpublished). Therefore we do not expect to operate at a baseline with slower response times than those reported herein.

Mode ‘Function modulation’ This mode was primarily designed to characterize eye movement responses to PAM, PRM or PAM/PRM. A sinusoid was chosen, because it is a smooth function without abrupt changes that could lead to patient discomfort.

Function modulation of PAM was fast and accurate. Quantization error could have been reduced, by selecting a smaller current range. The tradeoff would be a lower maximum output level. Function modulation of PRM was also accurate. Due to the non-linear pulse frequency resolution (500, 400, 333 pps etc.), any value between resolution steps was rendered on average through fast switching between adjacent pulse rates (e.g., Fig. 3.5C at 150 ms shows the

averaged pulse rate switching between 333 and 400 pps). At lower pulse rates, switching was slower because of the resulting lower update rate. For instance at 77 pps, the next change of pulse rate was applied 13 ms later (1/77 pps). This lower update rate explains the negative peak lags of 7 ms for 2 Hz and -4.5 ms for 5 Hz (e.g., steps in Fig. 3.5C,D). In the former case, the lowest pulse rate was in effect after the negative peak, whereas in the other case it occurred before. Therefore, the main contributor to RMSE_{QE} was the lower update rate, particularly below 100 pps.

Mode ‘Gyro modulation’ Gyro modulation performed well. In contrast to function modulation, gyro modulation was less jagged. Specifically for PRM, it did not show the clear pulse rate steps present with function modulation (Fig. 3.6F vs. Fig. 3.5D). This was due to response time jitter. For instance, the onset of the smallest pulse rate output had a standard deviation of 4.7 ms for FM 5 Hz in gyro modulation mode compared to 0.3 ms in function modulation mode. This small variance effectively smoothed the average responses in Fig. 3.6.

Latencies for positive and negative peaks for PAM were below the crucial threshold of 6.5 ms. This was partly true for the positive peak lag with PRM, results for the negative peak lag were larger than 10 ms and can be attributed to the lower update rate present at pulse rates below 100 pps.

The phase delay in PAM and PRM mode moved the output accordingly by the specified 50 ms, and otherwise did not change the characteristics of the signal. The delay could be used to better fit electrically evoked responses with natural VOR responses (arising from sensors with a known time constant).

The frequency of the input signal did not influence PAM output, RMSE_{QE} was zero. In PRM mode, however, the 5 Hz input frequency yielded lags like the 2 Hz case (high lags at low pulse rates), and consequently led to more than twice as high RMSE_{QE}. The errors for 5 and 2 Hz had a ratio of 2.6 (5/2 equaling 2.5).

RMSE_{QE} for gyro modulation PRM were larger than for function modulation. For 2 Hz function modulation it was 1.4 pps, for gyro modulation 7.9 pps. The error at lower pulse rates was exacerbated by the response time to the gyroscopic input which was disregarded during function modulation, illustrated by larger negative peak lags (7 vs. 13.9 ms).

Comparing PAM, PRM and PAM/PRM PAM, PRM, and PAM/PRM modulations are ready for operation. A thorough study is required to determine the most effective and efficient modulation paradigm in humans. Previous studies on

a human patient showed that PAM elicited slightly stronger eye movements than PRM, but both modes were not systematically compared and parametric changes were not exhaustive (Guyot et al., 2011).

One advantage of PRM may be lower current spread than with PAM. PRM alone has shown less misalignment of VOR in chinchillas (Davidovics et al., 2012) and rhesus monkeys with modified cochlear implants (Nie et al., 2013). The underlying hypothesis was that the total number of evoked action potentials influenced VOR. This number can be changed (in PAM) through recruiting more neurons with a higher pulse amplitude (thus increasing the risk of current spread), or (in PRM) by making already recruited neurons fire more often with a higher pulse rate.

However with PRM mode, two issues warrant highlighting: first, the non-linear pulse rate resolution, especially at high pulse rates, and second, the lower update periods leading to an error with decreasing input signals. It has to be noted, that the tested angular velocities were extremely high (-750 to 1000 °/s) and more than twice the value experienced with head impulse tests (Cremer et al., 1998) and much higher than angular velocities recorded during healthy locomotion that peaked at 140 °/s (Pozzo et al., 1995). Subjects with vestibular disorders are expected to experience lower angular velocities for activities such as running in light or darkness (Pozzo et al., 1991).

Regarding the first issue, it will be interesting to see whether subjects will be able to notice the fast switching between pulse rates like 222.2 and 250 pps. It is important to stress that these are instantaneous rates. Future perceptual tests should clarify the exact meaning of the PRM RMSE. Specifically, we will verify whether pulse rate is estimated by the vestibular system instantaneously (i.e. dt between the current and prior pulse) or in a longer history of multiple pulses through averaging. If the latter case held, this would effectively smooth the errors calculated herein.

The second issue will likely result in lower than expected inhibitory eye movement responses or asymmetry between excitatory and inhibitory responses; a problem witnessed with unilateral implants and physiological baseline stimulation rate that was not alleviated with chronic stimulation (Dai et al., 2011). Elevated baseline pulse rate evoked more symmetrical responses (Merfeld et al., 2007). That option and the possibility to set different gains for positive and negative angular velocities should be explored to produce symmetric eye movement responses. Bilateral implantation is another approach (Gong et al., 2008), but remains unlikely in humans due to the inherent risks of two surgeries.

The combination of PAM and PRM could also improve responses. Both could complement each other. It has been shown that co-modulation increased the range of eye movement responses (Davidocis et al., 2012, 2013). The authors suggested using co-modulation to provide a wide range of excitatory and inhibitory responses with a unilateral implant. However, this effect has yet to be shown in humans.

3.5 SUMMARY

We presented a system that can interface a 3-axis gyroscope sensor with a custom MED-EL cochlear-vestibular implant and is capable of modulating three independent stimulation outputs to angular velocities with a latency similar to natural VOR latency. The system offers tools for pulse amplitude and pulse rate modulation as well as a combination thereof. A second advantage is the computational power allowing for floating point calculation and for more complex transfer functions. Graphical user interfaces are the third main advantage letting the operator change parameters with ease while stimulation is active without the need to pause the stimulation (a critical feature to avoid nystagmus).

Patient trials with the system are ongoing and have focused first on the characterization of eye movement responses to function modulation of PAM and PRM. The outcome of these experiments is described in the following Chapter 4.

EFFECTS OF PULSE AMPLITUDE AND PULSE RATE MODULATION DURING ACUTE ELECTRICAL STIMULATION WITH A VESTIBULAR IMPLANT IN HUMAN PATIENTS

Abstract Patients instrumented with vestibular implants have shown preliminary encouraging results, but the different effects of stimulation strategies based on pulse rate (PRM) or pulse amplitude modulation (PAM) have not been yet identified. Here, we address this issue by acutely testing a vestibular implant in four bilateral vestibular loss subjects using either PAM or PRM.

At a super-physiological baseline pulse rate, PAM evoked stronger eye movement responses than comparable PRM. Lowering the baseline pulse rate significantly reduced the PAM response, but did not significantly change the PRM response.

We also developed a neural network model that simulated the implant interacting with the vestibular nuclei and reproduced the relationships from the clinical tests. This model revealed that PAM consistently causes greater changes in recruitment and firing rate than PRM due to both the initial adaptation to implant activation, and the interdependency of stimulation parameters and afferent resting discharge rate.

Our findings suggest PAM as the preferred strategy for initial activation in human vestibular implants. Chronic studies are necessary to reveal whether VOR plasticity can enhance the response to the vestibular implant.

4.1 INTRODUCTION

The vestibular system plays an essential role in everyday life. Being at the interface of sensory and motor systems, it contributes to various levels of nervous function. For example, the vestibulo-ocular reflex (VOR) drives stabilization of gaze during head motion, while other pathways influence postural control and spatial orientation. All these rely on the input from the peripheral vestibular organs in the inner ear. When vestibular function is lost bilaterally, patients typically suffer for instance from imbalance, impaired spatial orientation, or oscillopsia. The prognosis of bilateral vestibular loss (BVL) is bleak (Zingler et al., 2008), patients have a reduced quality of life (Guinand et al., 2012) and no adequate treatment option is available.

Research in animal models have partially restored vestibular function (Merkel and Lewis, 2012). Performance was typically quantified via the VOR response. Early experiments with patients demonstrated viability (Guyot et al., 2011a; Guyot et al., 2011b) and we recently reported single-axis VOR restoration (Perez Fornos et al., 2014) and VOR dependency on modulation frequency (Van De Berg et al., 2015). A vestibular implant (VI) could therefore prompt significant rehabilitation.

Prototypes in animal models have predominantly employed pulse rate modulation (PRM) to replicate primary afferents' natural spike rate modulation (Fernandez and Goldberg, 1971). Pulse amplitude modulation (PAM) and co-modulation of pulse amplitude and pulse rate also evoked considerable eye movements (Davidovics et al., 2010; Davidovics et al., 2012). The conundrum whether PRM or PAM is more effective has recently gained relevance as modified cochlear implants, which effectively use PAM to transmit sound information, have become available for vestibular stimulation.

To address this issue, we tested four patients with VIs based on modified cochlear implants providing independent electrodes to stimulate vestibular nerve branches. We characterized their eye movement responses to PAM and PRM during acute trials. Specifically, we injected equal amounts of charge with both paradigms to compare their efficacies. To unify the experimental results, we built a simple, but biologically inspired model of VOR driven by electrical stimulation. The model was adapted only to continuous baseline stimulation present at implant activation. It then reproduced the relationships between PRM and PAM found in acute experiments and provided interesting insights about possible results of chronic stimulation. Our findings indicate PAM as preferential paradigm – at least during the acute stage after implant activation.

4.2 METHODS

4.2.1 Patients

Experiments were performed in accordance with the Declaration of Helsinki. The ethics committees of the University Hospitals Geneva (NAC 11-080) and the Maastricht University Medical Center (NL36777.068.11/METC 11-2-031) approved this study.

Among a pool of eleven patients that received modified cochlear implants (MED-EL, Innsbruck, Austria), four patients were available for this study (named BVL1 – BVL4, Table 4.1). The stimulation sites were in proximity to the ampul-

iae of the lateral, superior or posterior ampullary nerve (LAN, SAN and PAN, respectively). Details on inclusion criteria, implant and surgical approaches have been published elsewhere (Van De Berg et al., 2012; Perez Fornos et al., 2014).

4.2.2 *Stimulation and Recording Paradigm*

Patients were tested acutely, 2-3 hours per electrode, and remained seated in a non-moving chair in a dark room. Stimulation was controlled with a customized system (Nguyen et al., 2014). The baseline pulse amplitude was set approximately in the middle of the dynamic range, i. e., between lower (vestibular) and upper (comfortable) thresholds (Perez Fornos et al., 2014). Baseline stimulation was maintained for 30 minutes for all vestibular symptoms such as nystagmus to subside (Guyot et al., 2011b).

All patients were tested at 200 pps baseline pulse rate and a phase width of 400 ms. BVL3 and BVL4 were further subjected to a 100 pps baseline pulse rate (same phase width). The rationale behind super-physiological baseline pulse rates is to create symmetric excitatory and inhibitory responses with a unilateral implant to compensate for bilateral loss. For PAM, pulse amplitude was sinusoidally modulated at a modulation frequency of 1 Hz. Medium and high levels of PAM were tested at 75 and 100% of the full dynamic range. A low setting at 50% dynamic range did not consistently evoke a significant response and is not presented.

For PRM, pulse rate was sinusoidally modulated to inject the equivalent charge as PAM (levels medium and high). Specifically, the injected charges by the cathodic phases during a half-cycle of the sinusoid were matched (Fig. 4.1A-F). With PRM, an additional level 2xhigh with doubled charge was applied.

Before modulation start, subjects focused for a few seconds on a LED in front of them. Afterwards the LED was turned off and eye movement responses were recorded with a bi-dimensional, monocular video eye tracking system (EyeSeeCam, Munich, Germany). Sixty modulation cycles were recorded for each trial in complete darkness. All settings are summarized in Table 4.1. Due to limited testing time, BVL4 was only subjected to high level stimulation.

4.2.3 *Analysis*

Data was analyzed post-hoc with Matlab 2013b (MathWorks, Natick, MA). Cycles with blinks or saccades were omitted. Total peak eye velocities (PEVs) were

then computed and normalized for comparison as explained in (Van De Berg et al., 2015). Statistical significance was tested with one-way ANOVA (Analysis of Variance).

Eye movement response axes were calculated with principal component analysis (PCA) of processed horizontal and vertical eye positions. Angles are given with respect to the first quadrant between 0-90°(horizontal axis 0°).

4.2.4 *Vestibular Nuclei Model*

We designed a simple model of the VOR pathway with the vestibular nuclei (VN) (Fig. 4.1G). The governing equations are listed in the Appendix. Briefly, acute activation of the implant caused a discontinuity that was modeled as a change of firing rate in afferents proximal to the electrode. We simulated 2000 afferents with a lower-than-physiological resting discharge at 30 Hz to emulate vestibular pathology (Fetter and Dichgans, 1996). The VN adapted to implant stimulation by attenuating synaptic weights of recruited afferents and increasing the offset that balanced all afferent input. Figure 4.1H shows afferent recruitment due to prosthetic stimulation. For PAM, increasing sub-populations of afferents were activated during up-modulation, while the inverse occurred during down-modulation. The pulse amplitude determined the radius of the sphere. In contrast, PRM always interacted with the same afferents because pulse amplitude was fixed. These afferents' firing rates were set by PRM.

Additionally, we simulated chronic stimulation performance and VOR learning based on retinal slip (Arnold and Robinson, 1997). Conceptually, the model learned from simulated head movement, which were sampled from a distribution reported for walking subjects with vestibular deficiency (Pozzo et al., 1991). The learning rate was identical for PAM and PRM. Similar to acute simulations, synaptic weights were adapted by back-propagation of least-means squares error. Other inputs for learning, such as cerebellum or neighboring brain stem nuclei, were intentionally neglected. We assumed their contributions would be equivalent for PRM or PAM.

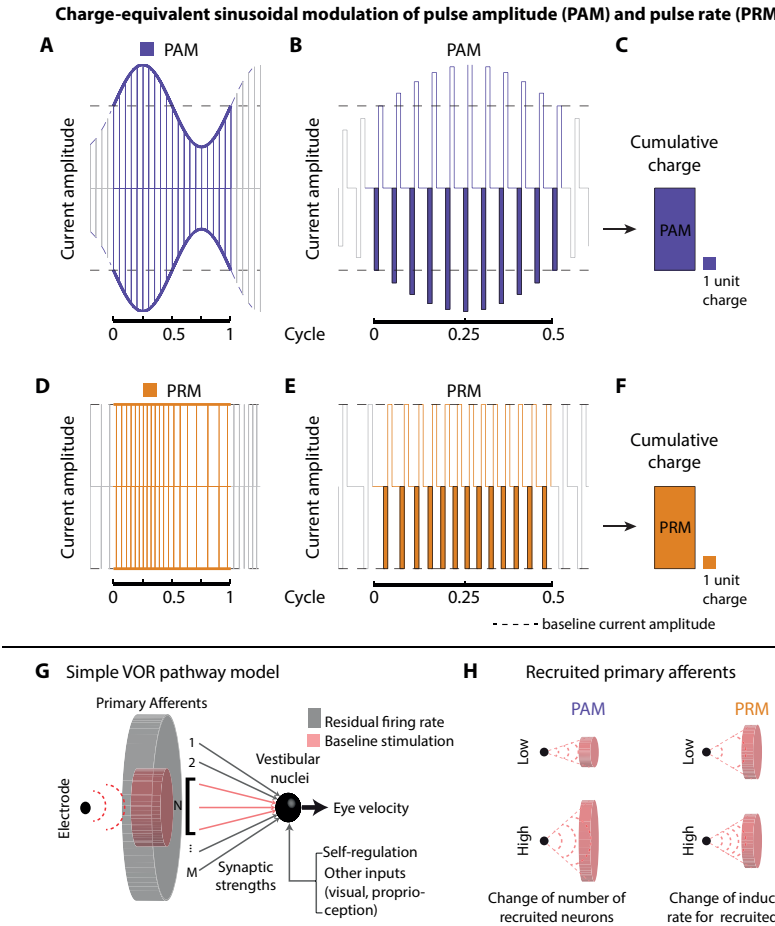


Figure 4.1: Visualization of charge-equivalent PAM and PRM, and the VOR pathway model. (A) PAM modulated the pulse amplitude and the intervals between pulses were constant (black dashed lines in plots denote baseline pulse amplitude). (B) Magnification of a half-cycle to illustrate individual pulses during PAM. The injected charge by the cathodic phases (purple areas) during one half-cycle were summed up (C) and PRM parameters were then matched to inject the equivalent charge during (D)-(F). Due to symmetry, it sufficed to compute the matched parameter for a half-cycle. Note how the intervals between pulses varied in (D) compared to (A). (E) Within a half-cycle, the PRM paradigm applied thirteen pulses at baseline pulse amplitude, while PAM applied eleven at different current amplitudes. (All plots are not drawn to scale for illustrative purposes.) (G) Illustration of the VOR pathway model. After vestibular injury, afferent neurons continue to fire at some or no resting discharge and are unresponsive to rotational inputs. These afferents synapse directly on the vestibular nuclei; thus have synaptic weights. These weights and any self-regulation must have adapted to equilibrium such that nystagmus is reduced to zero. At the moment the implant is turned on, a discontinuity is introduced. Specifically, there is a sub-population of neurons (red) suddenly firing at baseline pulse rate. We modeled this system as a linear summation (see Appendix). (H) Illustration of the two stimulation paradigms: PAM changes the size of the electric field and thus the number of recruited neurons firing at the baseline pulse rate, whereas PRM does not change the number of recruited neurons, but changes the induced firing rates.

4.3 RESULTS

4.3.1 Peak Eye Velocities

Figure 4.2 shows normalized peak eye velocities (PEVs) of the eight electrodes that evoked eye movement responses. Across all patients, PAM resulted in significantly higher responses than PRM at a baseline pulse rate of 200 pps.

Modulation levels had no consistent impact (Fig. 4.2A). High PAM evoked a significantly stronger response than medium PAM in one case (BVL1 SAN). For PRM, a response increase with modulation depth was only observed in BVL3 SAN, a decrease was seen in BVL2 SAN (both non-significant). For other electrodes, modulation levels had a mixed (small) effect on PRM responses.

BVL3 and BVL4 were additionally tested at a lower 100 pps baseline pulse rate (Fig. 4.2B). This led to a significant reduction for PAM, while PRM responses did not change significantly.

4.3.2 Response Axes

Figure 4.3A gives PAM and PRM response axes for LAN electrodes. Activation of these should ideally evoke horizontal eye movement (angle close to 0°) and high PRM resulted in response axes closer to 0° than high PAM.

For different modulation levels, PRM response axes did not significantly change (Fig. 4.3B). For BVL1 and BVL3 LAN, medium to 2xhigh PRM response axes showed a small, non-significant decrease.

PAM response axes changed significantly with modulation levels for BVL1 and BVL2. Medium PAM axes were closer to 0° (improvement of 45% and 79%, respectively).

Halving the baseline pulse rate to 100 pps moved PAM response axes closer to 0° (e.g., 33.2° to 10.4° for BVL3). PRM response axes did not change for BVL3, whereas for BVL4 a significant increase from 7.8° to 21.7° was observed.

For the SAN and PAN electrodes, response axes for PAM and PRM were markedly more vertical (angle closer to 90°) than for LAN electrodes (Fig. 4.3E). Only the axes for BVL3 stayed relatively horizontal (33.5° to 44.1°). Modulation levels had no significant effect on SAN and PAN response axes.

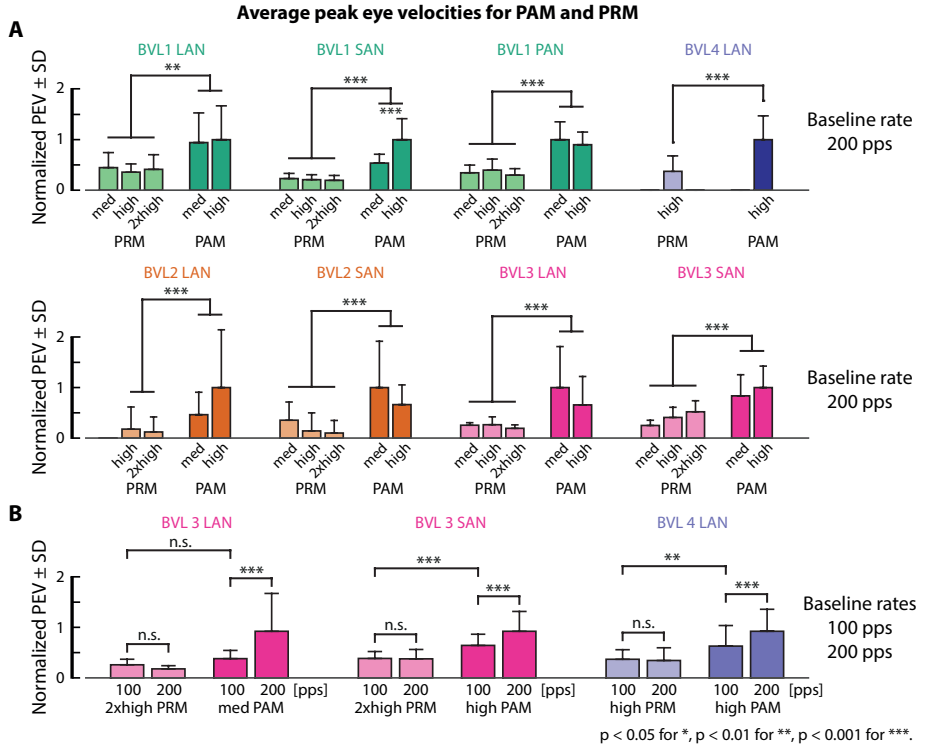


Figure 4.2: Average peak eye velocities (PEV) in response to PAM and PRM. (A)-(B) Normalized PEV for different modulation depths at a baseline pulse rate of 200 pps. Eight out of twelve implanted electrodes evoked eye movement responses. For all electrodes, PAM yielded significantly stronger responses than PRM ($p < 0.05$). Modulation depth did generally not significantly alter PEVs, except for PAM of BVL2 SAN. (Medium PRM for BVL2 LAN is excluded as it failed to show a response significant from zero.) (C) BVL3 and BVL4 were subjected to the lower baseline pulse rate of 100 pps resulting in reduced PEV for PAM. PRM responses were not significantly changed. For all tests, normalization to the strongest eye movement response, and one-way ANOVA.

EFFECTS OF PULSE MODULATION DURING ACUTE VI STIMULATION

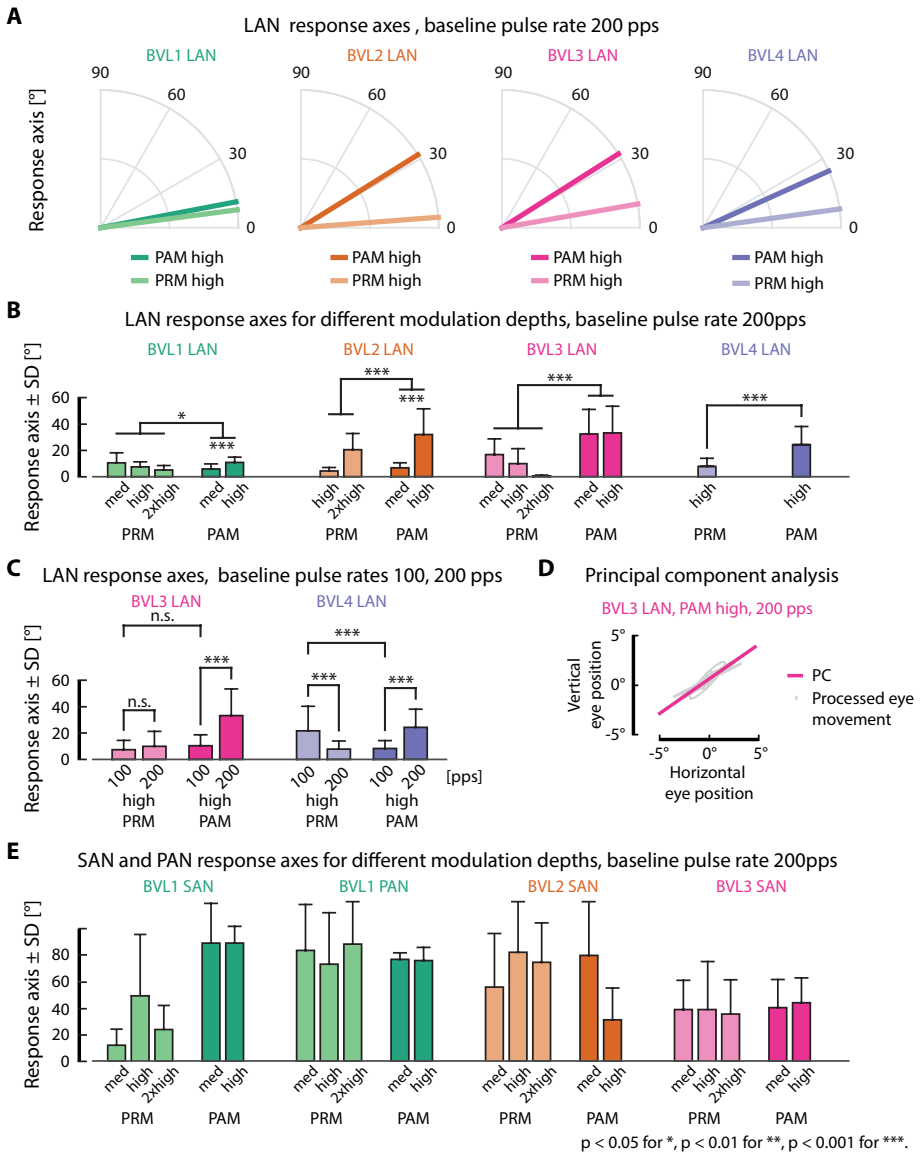


Figure 4.3: Eye movement response axes to PAM and PRM with principal component analysis (PCA). (A) Response axes to high level PAM and PRM for the four patients. PRM yielded axes closer to the ideal, horizontal axis in all patients. (B) Modulation depth had a mixed effect on PRM response axes; PAM response axes improved significantly for BVL1 and BVL2. (C) At a lower baseline pulse rate of 100 pps, PAM yielded responses closer to the horizontal axis than at 200 pps. PRM response axes were worse than at 200 pps for BVL4, but not for BVL3. (D) Processed vertical and horizontal eye positions (in grey) for a given modulation were used to calculate the principal component (PC, magenta line), here as an example in BVL3. (E) PAM and PRM response axes for other electrodes. Axes were more vertical than for LAN stimulation as expected. However, a comprehensive comparison was not feasible, since torsional eye movement – that are also expected with SAN and PAN stimulation – could not be recorded with our eye tracking system.

4.3.3 Vestibular Nuclei Model

First, we simulated the experimental tests at 200 pps baseline pulse rate of BVL3 LAN (largest absolute PEVs across all electrodes). We found clear differences in the resulting recruitments and ensemble firing rates (Fig. 4.4A-B). This resulted from PAM recruitment being a function of pulse amplitude and the discontinuity between baseline pulse rate and afferent resting discharge. With baseline stimulation, the synaptic weights of recruited afferents decreased compared to non-recruited ones (Fig. 4.4C). Thus action potentials during PAM passed through higher average synaptic weights than PRM.

Simulating different modulation levels, PAM generated larger eye movement than PRM (Fig. 4.4D). There were differences within each modality, but the largest change (37.5%) in pulse rate only generated approximately one-half the eye movement of the smallest change (16.7%) in pulse amplitude.

Reducing the baseline pulse rate to 100 pps changed the adapted synaptic weights and reduced the discontinuity in PAM. As in the experimental results, this caused no change in PEVs for PRM, but reduced PEVs for PAM (Fig. 4.4E).

Simulating adaptation to chronic stimulation predicted significantly faster convergence for PAM than PRM (Fig. 4.4F-G). PRM required on average 50% more steps, but had significantly lower final error. Across head velocities, PRM produced consistently low retinal slip. In contrast, PAM showed large slip for head velocities above 35 °/s, which engaged rarely updated synaptic weights (Fig. 4.4H).

4.4 DISCUSSION

We acutely tested PAM and PRM in four BVL patients with a VI. Across all responsive electrodes, PAM evoked clearly stronger PEVs than PRM. Although PRM had LAN response axes significantly closer to ideal than PAM, PEVs are more critical since studies have shown that misalignment could be managed. Therefore, PAM should be considered as preferential paradigm for initial VI activation.

4.4.1 Effects of Pulse Modulation on Response Axes

For LAN stimulation at 200 pps baseline pulse rate, PRM generally resulted in response axes significantly closer to the ideal horizontal axis than PAM. The size of the electrical field induced by PAM should be modulated, thus possibly

EFFECTS OF PULSE MODULATION DURING ACUTE VI STIMULATION

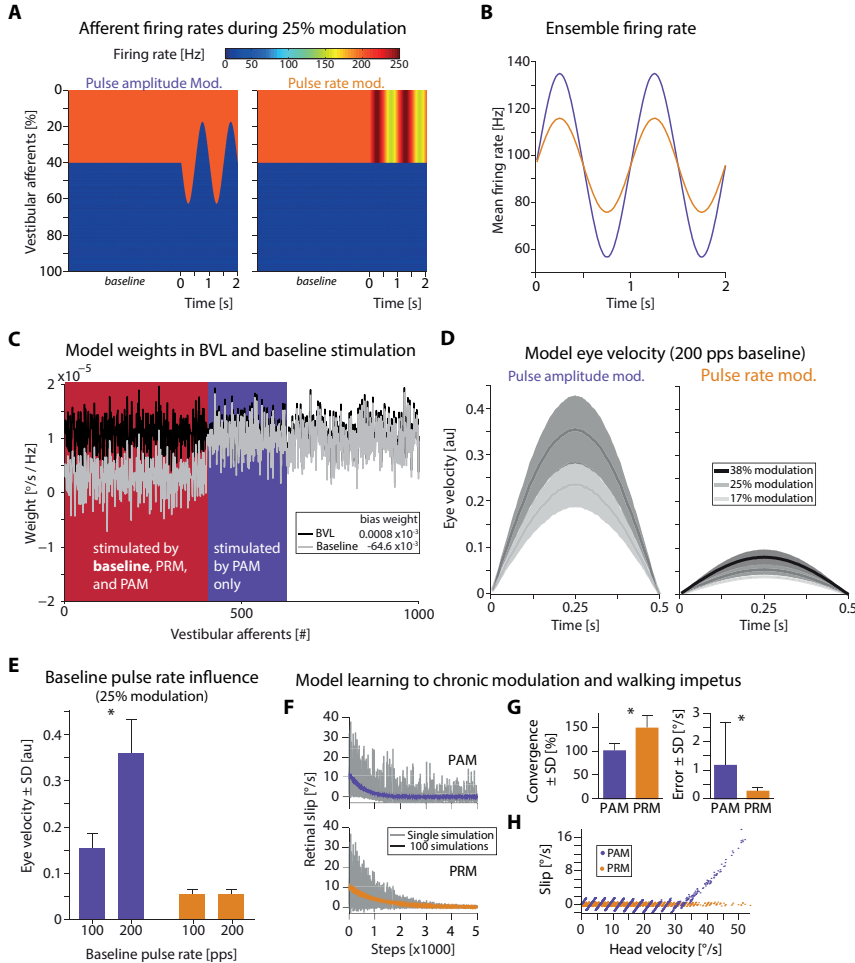


Figure 4.4: Simulation results with the vestibular nuclei model. (A) Application of charge-balanced PAM and PRM recruited different afferent sub-populations. (B) Averaging across all afferents, PAM induced a higher ensemble firing rate. (C) After vestibular injury, synaptic weights were determined by the resting discharge of each afferent. We used a distribution of resting discharge (26.3 ± 6.6 Hz); thus the initial weights were also distributed. When the implant was turned on, there was an induced error. (D) Mean eye response to PAM (17 and 25% modulation) and PRM (17, 25, and 38% modulation) for 50 cycles; bands are standard deviation. Since experimental PEVs were obtained during increasing pulse amplitude or pulse rate, we focused on the positive model output. (E) Model eye velocity was dependent on baseline pulse rate for PAM. PRM was not affected. (F)-(H) Simulation of chronic performance for both stimulation paradigms. (F) Walking was used as an impetus for retinal slip. Both single and mean ($n = 100$) simulations showed that PAM converged to less than $1^{\circ}/\text{s}$ retinal slip significantly faster than PRM (at 200 pps baseline pulse rate). (G) However, PRM eventually converged to a less variable and significantly lower final value of error. (H) Simulated slips from converged models found that PAM errors were higher for all velocities, especially apparent above $35^{\circ}/\text{s}$. (Bar plots are concatenated from 100 simulations, * is two-sample t-test, $p < 0.05$)

recruiting afferents in an adjacent canal, specifically SAN, which presumably would evoke non-horizontal eye movement. Indeed, high PAM in BVL1 and BVL2 had response axes significantly further away from ideal than medium PAM. With PRM, in contrast, the size of the electrical field should remain unchanged and modulation levels did not affect response axes. Our results were in agreement with findings in chinchillas, where PRM response axes were also closer to reference axes than PAM ones (Davidovics et al., 2012).

For a VI to be ultimately useful to patients, it should compensate for all head movements in 3D space. Response axes observed in BVL1 and BVL2 were encouraging in this respect, since LAN and SAN stimulation evoked eye movements predominantly in the horizontal or vertical directions, as expected from physiology. However, some misalignment could be observed. Studies demonstrated that initial misalignment to an ideal axis was significantly reduced over one week of continuous stimulation (Dai et al., 2013). This improvement has been attributed to the plasticity of the vestibular-ocular central nervous system, capable of adapting to activation patterns induced by an implant. Additionally, a coordinate transformation could reduce alignment (Fridman et al., 2010).

4.4.2 Effects of Pulse Modulation on Peak Eye Velocity and VN Model

In VIs for animal models, PRM has often been selected as encoding scheme to mimic the primary vestibular afferents' spike rate modulation (Merfeld and Lewis, 2012). However, PAM also elicited viable eye movement responses in patients (Guyot et al., 2011b) and has recently become more relevant as stimulation paradigm with the more widespread adoption of modified cochlear implants for vestibular stimulation (Valentin et al., 2013; Golub et al., 2014; Perez Fornos et al., 2014). Our findings revealed PAM's capability to evoke strong eye movements. Furthermore, they demonstrated that PAM was more charge-efficient than PRM, potentially extending battery life.

Modulation levels had generally no effect on PAM PEVs, most likely due to small increments between medium and high PAM in our subjects (modulation depths less than 30%). PEVs significantly increased with modulation depth only for BVL1 SAN for unknown reasons. These differences in PEVs across electrodes highlight the need for a better understanding of the underlying subject-specific pathologies to potentially adjust electrode design, electrode placement and to optimize modulation range. The insensitivity of PRM PEVs for different modulation levels, even at 2xhigh, may be due to the high baseline pulse rate.

For baseline pulse rates 100 and 200 pps, PEVs to PRM were practically identical, while PAM elicited stronger responses at the higher baseline pulse rate. A similar effect with higher baseline pulse rates favoring PAM was reported in chinchillas (Davidovics et al., 2012) and rhesus monkeys (Davidovics et al., 2013).

The VN model revealed the different efficacies for charge-balanced PRM and PAM. First, PAM recruited additional sub-populations of afferents and triggered a sharp change in firing rates from resting discharge to the higher, induced pulse rate. Second, these sub-populations had greater synaptic weights, as they were not attenuated by adaptation to baseline stimulation. Engaging these weights, therefore, led to significantly larger PEVs with PAM than with PRM. In contrast, PRM was confined to the same sub-population with attenuated weights and had no access to sub-populations with greater weights. These mechanisms also revealed that PAM was strongly dependent on the baseline pulse rate, while PRM had minimal dependency, as found in our experiments.

Chronic stimulation in patients was not approved at the time of this study. Evidence from animal research suggests that chronic stimulation could improve responses. Chronic PRM responses improved significantly during continuous stimulation (90 days) at baseline pulse rates above 200 pps, likely due to VOR learning (Lewis et al., 2010). To our knowledge chronic PAM studies in animal models have not been reported. It is therefore possible that PAM responses could improve chronically, too.

The VN model also simulated chronic stimulation and adaptation. These simulations highlighted effects of PRM and PAM engaging different afferent populations. PAM generated larger PEVs and thus larger retinal errors, which facilitated learning. However, this learning was inconsistent as synaptic weights for rarely sampled high head velocities were updated rarely (Fig. 4.4H). In contrast, PRM continuously updated the same synaptic weights and learned a lower error solution across all head velocities.

4.5 SUMMARY

Our experimental findings and model simulations strongly support PAM at 200 pps baseline pulse rate as preferential acute stimulation paradigm. The findings add urgency to investigate chronic stimulation with PAM, as its chronic efficacy remains an open issue.

APPENDIX – SUBJECT DETAILS

Table 4.1: Patient demographics and stimulation parameters. Cursive printed modulation depths denote setting for largest eye movement response for corresponding electrode.

Patient	Sex, etiology	Age at implantation, implanted ear	Electrode	Baseline pulse rate [pps]	Baseline pulse amplitude [μ A]	Level	PAM [$\pm\mu$ A], (modulation depth)	PRM [\pm pps], (modulation depth)	Largest electrode response [$^{\circ}$ /s]			
BVL1	Male, DFNA9	66, left	LAN	200	200	medium	15 (7.5%)	10 (5%)	1.8			
						high	25 (12.5%)	20 (10%)				
						2xhigh	40 (20%)					
			SAN	200	155	medium	15 (9.7%)	22 (11%)	4.9			
						high	25 (16.1%)	29 (14.5%)				
			PAN	200	200	2xhigh	38 (19%)	37 (18.5%)	3.6			
BVL2	Female, DFNA9	68, left	LAN	200	300	medium	56 (28%)	55 (27.5%)	1.4			
						high	112 (56%)					
			SAN	200	350	2xhigh	25 (8.3%)	16 (8%), no response	1.2			
						high	50 (16.7%)	34 (17%)				
						2xhigh	50 (25%)		1.2			
						medium	34 (9.7%)	18 (9%)				
						high	50 (14.3%)	27 (13.5%)	1.2			
						2xhigh	84 (42%)					

Patient	Sex, etiology	Age at implantation, implanted ear	Electrode	Baseline pulse rate [pps]	Baseline pulse amplitude [μ A]	Level	PAM [\pm μ A], (modulation depth)	PRM [\pm pps], (modulation depth)	Largest electrode response [°/s]
BVL3	Female, trauma	67, left	LAN	200	300	medium high 2xhigh	50 (16.7%) 75 (25%)	34 (17%) 50 (25%) 75 (37.5%)	7.8
			LAN	100	300	medium high 2xhigh	50 (16.7%) 75 (25%)	36 (36%) 72 (72%)	1.2
			SAN	200	400	medium high 2xhigh	50 (12.5%) 75 (18.8%)	26 (13%) 39 (19.5%) 80 (40%)	4.0
			SAN	100	350	medium high 2xhigh	50 (14.3%) 100 (28.6%)	27 (27%) 54 (54%)	1.2
BVL4	Male, DFNA9	66, left	LAN	200	120	medium	60 (50%)	100 (50%)	7.6
			LAN	100	120	medium	60 (50%)	50 (50%)	2.8

APPENDIX – VESTIBULAR NUCLEI MODEL EQUATIONS

- Model specification, i. e. before stimulation onset

$$v = \tanh \left(\sum_N w_i x_i + b \right) = 0$$

- Output at VI activation, baseline stimulation

$$v = \tanh \left(\sum_N w_i \textcolor{red}{x_i} + b \right) \neq 0$$

- Adaptation to minimize nystagmus

$$\begin{aligned}\epsilon &= 0 - v \\ \delta w_i &= \alpha_w e (1.1 - v^2) x_i \\ \delta b &= \alpha_{\text{bias}} e (1.1 - v^2)\end{aligned}$$

where v is peak eye velocity output, N the total number of afferents, w_i their synaptic weights, x_i the afferents' spontaneous or induced firing rate, b the bias term. Before stimulation onset, at rest, afferents are firing at their spontaneous resting discharge rate and v is zero. The tanh function introduces a linear and saturated regions that replicate natural behavior.

When baseline stimulation is activated, a number of afferents is recruited by the stimulation and their firing rate x_i will change. This results in eye movement that contradicts the stationary visual surrounding (subject sitting in a chair). The resulting error e is minimized to zero through adaptation of synaptic weights and the learning rates α_w , α_{bias} for the afferents and bias, respectively.

Part II

VECAP – VESTIBULAR ELECTRICALLY EVOKED COMPOUND ACTION POTENTIAL

ARTIFACT REDUCTION FOR VECAP MEASUREMENT

Abstract In the clinic, vestibular function is commonly evaluated through eye movement responses. These eye movement responses are also used for the assessment of vestibular implant performance. Additional objective metrics, such as vestibular electrically evoked compound action potentials, may provide useful information. VECAPs have been reported before as a tool for electrode placement during surgery and were recorded with a modified cochlear implant. Here, we recorded VECAPs with a custom, double-sided electrode array in the ampulla of a guinea pig. Phase width had to be shortened to 25 µs compared to the typical phase width of 200 µs. The masker-probe technique reduced artifact and yielded VECAP comparable to literature. An artifact template was also created and could serve as a proxy for the full masker-probe paradigm.

5.1 INTRODUCTION

In Chapter 4 we evaluated the effects of pulse amplitude and pulse rate modulation through the eye movement response. It is regarded as the most objective measurement of vestibular function. Perceptual or balance tasks could also be used for assessment. However, they additionally engage other sensory inputs such as vision or proprioception and therefore do not test vestibular function alone. In fact, some patients learn to compensate to some degree through other sensory inputs (Curthoys, 2000).

VECAPs may be an additional objective and exclusive metric of vestibular function. Generally in ECAP recordings, a measurement electrode is located extracellular, outside nerve fibers, and close to the source of electrical stimulation. Stimulation then induces synchronized action potentials in afferents and the measurement electrode records the sum of their voltage change (compound action potential). Recording of non-synchronized action potentials (i.e., spontaneous firing) would be on average not significantly different from zero.

VECAPs would provide direct recording of the peripheral vestibular nerve before any central processing. Auditory ECAPs have been studied more extensively with cochlear implants, often with the objective to estimate implant performance or for fitting stimulation thresholds (e.g., Abbas et al., 1999; Bah-

mer et al., 2010). Auditory ECAPs have typically a duration of one millisecond and exhibit first a negative wave (N) and then a positive wave (P) (cf. Fig. 2.2D).

So far, VECAPs were reported as tool to improve electrode placement for a vestibular implant in rhesus monkeys (Nie et al., 2011). VECAPs had similar characteristics and waves compared to auditory ECAPs. In that study, obtaining peri-operative VECAPs was generally also predictive of post-operative eye movement responses to electrical stimulation. However, the group had difficulties to reproduce these results in human patients (Golub et al., 2013).

VECAPs could also be utilized for fitting of stimulation thresholds, similar to cochlear implants. We additionally believe that it could be used as feedback signal for a closed-loop VI that could potentially improve VI performance. Here, we present methods to acquire VECAPs with a custom, double-sided electrode array with eight active sites (Poppendieck et al., 2014). This design is markedly different from the electrode array of cochlear implants, that have electrode sites inside a silicone rubber tube. Yet techniques known from auditory ECAP recording were used with adjustments.

5.2 METHODS

Animals and surgery

One male, adult guinea pig was used for this study. The institutional animal care and use committee approved all experiments. In the first of three surgeries, the subject was instrumented with a fiberglass-composite structure ('headbolt') and a container for stimulation circuitry and connectors ('headcap'). Second, a 3-turn stainless steel eye coil was inserted into the left eye for eye movement recording. Third, the double-sided electrode array with four sites each was implanted in the ampulla of the left horizontal canal. The electrode sites on the array were numbered as follows: 1-3-5-7 on the top side, 2-4-6-8 on the bottom side. The tip of the array had a width of 245 µm and a length of approx. 1.2 mm. A remote electrode was inserted into the neck muscle. The position of the array was checked during surgery with a portable stimulator and by monitoring eye movement. Details about the surgeries have been published elsewhere (Merfeld et al., 2006).

Stimulation and recording paradigm

Stimulation and recording were applied with a MED-EL Research Interface Box II (RIB2, Innsbruck, Austria). Corresponding scripts were programmed in Matlab (Mathworks, Natick, MA, USA). The setup is illustrated in Fig. 5.1.

The RIB2 provided voltage measurements with a resolution of 5 µV at a sampling rate of 1.2 million samples per second (every 0.83 µs). Each recording had 2048 samples, approx. 1.7 ms. The samples were converted from analogue values to a digital sequence with an adaptive sigma-delta modulation (Zierhofer et al., 2000) and afterwards demodulated post-hoc with a Matlab script. Measurements were averaged over 25 iterations.

To achieve VECAP recording several steps had to be performed, outlined below.

Threshold identification Two weeks after the third surgery, thresholds were obtained for all eight electrode sites with the electrode in the animal's neck muscle serving as return electrode. Phase widths were 200 µs with a phase gap of 2.1 µs (minimum setting in RIB2). Pulse trains with 20 pulses at 250 pps were applied and the animal was held by a second experimenter who monitored eye movement responses. Pulse amplitudes were increased in steps of 10 µA for each train. The lowest pulse amplitude that evoked an eye movement was set as vestibular threshold (THR). The pulse amplitude that first activated the facial nerve and resulted in facial twitching was set as most comfortable level (MCL).

Electrode site 4 was chosen for the remainder of the study with a lower threshold at 60 µA and no MCL. The results for all eight electrode sites are not reported herein for space.

Monopolar, bipolar stimulation and recording First, the aim was to record the nerve response to a single stimulation pulse, intentionally prior to any artifact reduction. Stimulation with electrode site 4 was monopolar or bipolar, i. e. the return electrode was the remote electrode in the neck or an electrode site on the array, respectively. Accordingly, recording was tested monopolar or bipolar. If both stimulation and recording were done bipolar, then the remote electrode was used by both.

The stimulation was applied with a single pulse, pulse amplitude was 70 µA and phase width 200 µs. At the time of the study, the hardware did not facilitate multipolar stimulation or recording and would have been beyond the scope of this pilot study.

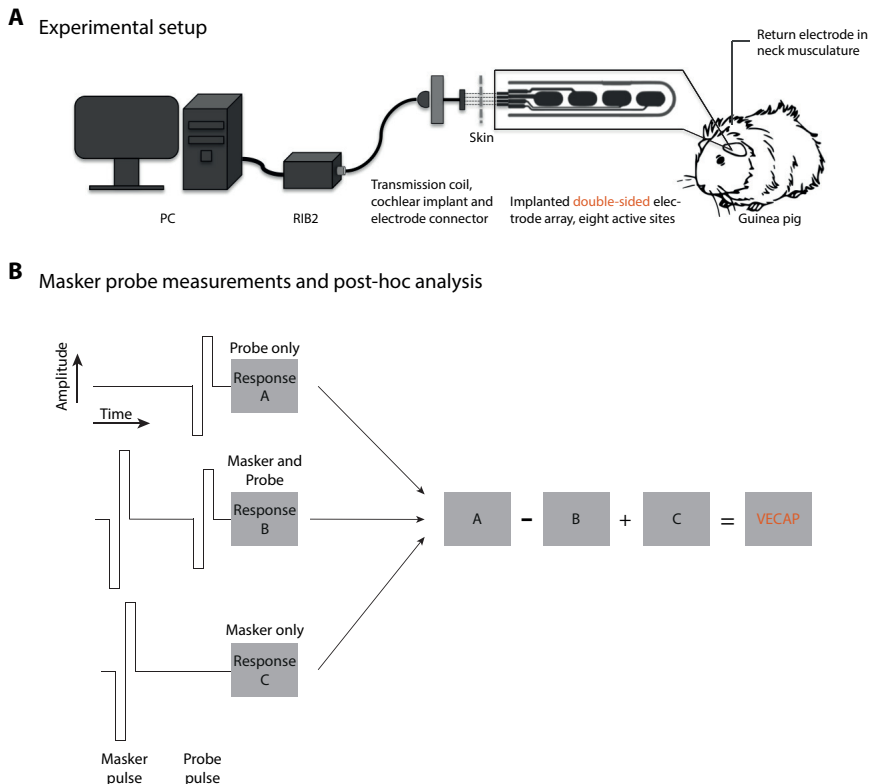


Figure 5.1: Setup for VECAP recording. (A) A PC was connected to a Research Interface Box (RIB2) that executed stimulation and recording. Data were sent and received with the RIB2 through a transmission coil connected to a cochlear implant outside the animal. The implant was connected to the implanted electrode array through a transcutaneous cable. The animal had been instrumented with the double-sided electrode array (sketch shows one of the symmetric sides) in the left ear. A return electrode was inserted into the neck musculature. (B) The masker-probe paradigm to measure VECAP. Three sets of pulses are applied that yield responses A, B, and C. Response A contains the targeted neural response to the probe pulse, but is also contaminated by stimulation artifact to the probe pulse. Using responses B and C and exploiting the neurons' refractory period, one can calculate post-hoc VECAP as shown.

Stimulation was applied through electrode site 4 and the recording through electrode site 3. The return electrode for monopolar configuration was the electrode located in the neck muscle. For bipolar configuration, electrode site 8 on the array was chosen arbitrarily as a first guess.

Variation of phase width and measurement delay Second, the phase width was varied between 25 and 200 μs with stimulation and recording electrode sites determined from the previous step. 200 μs had been the typically used phase width in VI research. The measurement delay, i. e. the delay between beginning of stimulation pulse and measurement start, was also varied up to 600 μs from the RIB2 minimum (two times phase width plus phase gap and plus 50 μs). However, this compulsory blanking period to avoid amplifier saturation did not yield improvements. Therefore, recordings herein are reported for the minimum measurement delay.

Combination of recording sites Third, all bipolar recording combinations were tested for monopolar stimulation of electrode site 4. For instance, recording was done with electrode site 1 and electrode site 8 as measurement return. This yielded 42 combinations in total. Specifically, recording with electrode site 1 to electrode site 8 was not considered as mirrored recording of electrode site 8 and electrode site 1 as return.

Artifact reduction Fourth, having identified suitable electrode sites for stimulation and recording as well as phase width, artifact reduction techniques were applied. These stimulation artifacts arise due to the spatial proximity of electrode sites, thus resulting in a recording electrode site measuring partial stimulation *signal* and not solely stimulation *response*.

In cochlear implants, the masker probe with three parts is a standard procedure (cf. Fig. 5.1). Three pulses are applied: (i) the probe pulse only, (ii) masker and probe pulses together with a distance of 300 μs and masker pulse amplitude 10 μA larger than the probe pulse amplitude, and (iii) the masker pulse only. The response to (i) contains the neural response to the probe pulse and the artifact to that pulse (response A). The response to (ii) contains the neural response to the masker pulse and artifacts of both the masker and probe pulses (response B), but not a neural response to the probe pulse. The masker pulse triggers an action potential in afferents first. These are then unable to respond again to the probe pulse since they are in an absolute refractory state (400 μs). The response to (iii) contains the neural response to the masker pulse and the artifact of the masker pulse (response C). To obtain the neural

response to the probe pulse, one has to subtract response B from response A and add response C.

We compared the masker-probe technique with two other techniques. The probe artifact template learned a probe artifact from recordings from a different day. The sub-threshold template learned an artifact template from recordings below averaging three lower threshold recordings and scaled it linearly with pulse amplitude (Nguyen et al., 2011).

Amplitude growth function Finally, VECAPs were recorded with the aforementioned artifact reduction techniques for fourteen different pulse amplitudes.

5.3 RESULTS

5.3.1 *Stimulation Settings*

Figure 5.2 shows the four combinations of monopolar and bipolar stimulation and recording.

Monopolar stimulation above the threshold resulted in an eye movement response, bipolar stimulation (return with electrode site 8) did not yield eye movement responses, even at the maximum pulse amplitude imposed by the stimulator ($750 \mu\text{A}$).

Monopolar recording had a small inflection around $500 \mu\text{s}$ and then returned to 0 V . (Times are given from pulse onset.) However, monopolar stimulation and recording shared the same return electrode which may introduce difficulties in later studies.

Bipolar recording of monopolar stimulation experienced saturation that lasted until $600 \mu\text{s}$. Bipolar recording of bipolar stimulation showed a rise to a constant level that indicated saturation of the amplifier.

For subsequent tests, monopolar stimulation and bipolar recording were chosen as they had the most promising measurement. To alleviate amplifier saturation, the phase width was decreased from the typically used $200 \mu\text{s}$ to $25 \mu\text{s}$. Figure 5.3 illustrates the effect of the shorter phase widths. The saturation is first shortened and eventually does not affect the $25 \mu\text{s}$ measurement.

Continuing with $25 \mu\text{s}$, all 42 bipolar recording combinations were tested for monopolar stimulation with electrode site 4. Specifically, measurements were taken with electrode site 1 and return with electrode site 8, or in short notation 1-8, continuing with 1-7, 1-6 etc.. The pair 8-5 was the combination

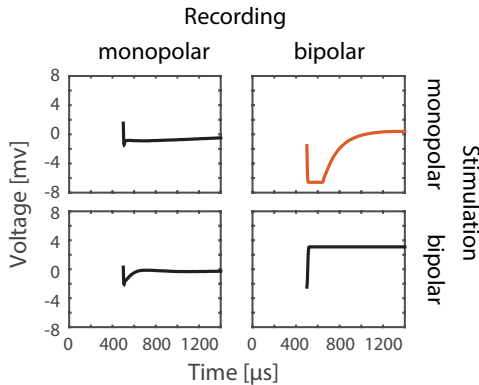


Figure 5.2: Monopolar and bipolar stimulation and recording. Plots show the measurement to a single pulse applied through electrode site 4. Bipolar stimulation did not yield a physiological eye movement response, and was not further pursued. With monopolar stimulation, monopolar recording had a short spike, while bipolar recording yielded amplifier saturation. Despite the saturation, monopolar stimulation and bipolar recording was the most encouraging configuration (red).

that resembled VECAP and auditory ECAPs from literature. This pair was used afterwards for artifact reduction.

5.3.2 Artifact Reduction Techniques

Artifact reduction was performed with the standard masker-probe technique and compared to templates derived from data either from an earlier day (probe artifact template) or sub-threshold measurements. Figure 5.4A-C shows the

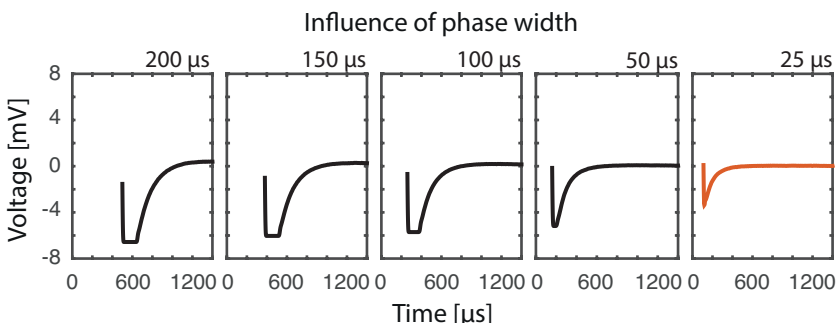


Figure 5.3: Effect of phase width on recording. The usually applied $200\ \mu s$ phase width resulted in clear amplifier saturation. Reducing phase width shortened the duration of saturation and ultimately at $50\ \mu s$ and $25\ \mu s$ resulted in measurements without saturation (red).

responses A, B, and C. Responses B and C had larger voltages than response A due to the added response components of the masker pulse.

The probe artifact (subtracting response C from response B) or the probe artifact template were similar in shape in size. In contrast, the sub-threshold template had a different shape, already similar to an actual VECAP recording (Fig. 5.4D-F).

Subtracting the artifact (template) from the response A yielded VECAP measurements for the three techniques. Both probe artifact and the probe artifact template showed a VECAP with a (sharp) negative wave and a positive wave. Instead, VECAP calculated with the sub-threshold template had only a positive peak (Fig. 5.4G-I).

The amplitude growth function (AGF) reports the dependency of N-P voltage in VECAP for different probe pulse amplitudes (Fig. 5.4J). For the probe artifact, AGF increased almost linearly up to 600 μ A and then flattened. A similar AGF was measured for the probe artifact template (no measurements larger than 600 μ A). The AGF of the sub-threshold template was lower than the other two and did not flatten, but kept increasing beyond 600 μ A. Since the VECAP did not have a negative wave, the P value was used for the AGF.

5.4 DISCUSSION

VECAP was successfully obtained with a custom, double-sided electrode array implanted in the semicircular canal of a guinea pig. Different stimulation configurations were tested and VECAP was recorded with artifact reduction techniques showing similarities with VECAPs and auditory ECAPs from the literature.

Protocol for VECAP acquisition Monopolar stimulation resulted in clear eye movement responses that a second experimenter qualitatively observed while holding the animal. This was expected as one can assume a larger electrical field due to the distance of the return electrode in the neck muscle. In contrast, bipolar stimulation used two electrode sites on the electrode array and no eye movement response was observed, even for maximal pulse amplitudes. Although bipolar stimulation may offer more selective and specific stimulation through a smaller electric field, it was not pursued any further since no eye movement response could be observed.

Monopolar recording of monopolar stimulation shared the identical return electrode. Contrary to expectation, this did not lead to amplifier saturation. However, no clear response was seen in the measurement (Fig. 5.2). Bipolar

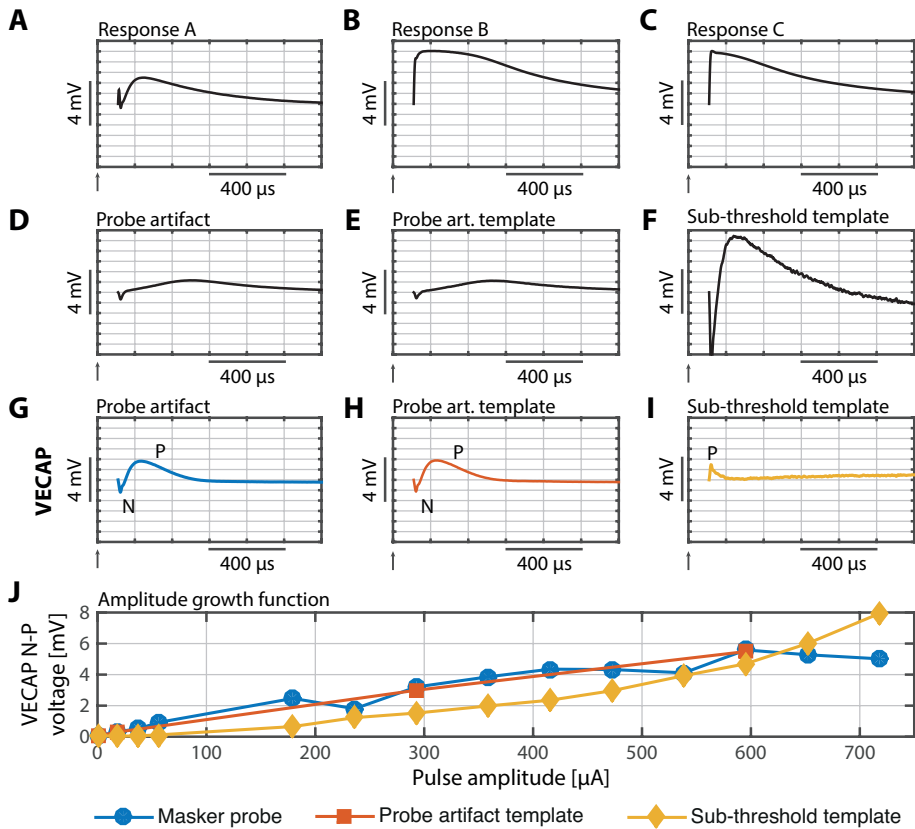


Figure 5.4: Artifact reduction for VECAP recording. (A-C) Responses A, B, and C for the masker-probe paradigm (cf. Fig. 5.1B). Small arrows indicate stimulation onset. (D-F) The three different probe artifacts. Note the distinct difference between probe artifact, probe artifact template and on the other hand the sub-threshold template. (G-I) Resulting VECAP for the three different techniques. VECAP with probe artifact and probe artifact template had negative and positive waves. VECAP with sub-threshold template had only a positive wave. (J) The amplitude growth function reporting the dependency of VECAP on pulse amplitude. Similar behavior again for probe artifact and probe artifact template; both had a linear increase up to 600 μ A. Sub-threshold template gave rise to a function that first had lower values than the other two, but then had no flattening at high pulse amplitudes.

recording, on the other hand, led to amplifier saturation, but a negative wave was visible and therefore further pursued.

To reduce stimulation artifact, phase width was reduced. A short phase width of 25 μ s was then chosen for further measurements. This phase width was considerably shorter than the phase width typically used in vestibular implants for animal models or patients (200 μ s). But it was more similar to phase widths used in cochlear implants (e.g., 30 μ s). In fact, this could mean that the pulse rate may have to be increased for vestibular implants to achieve a comparable eye movement response to the response with 200 μ s phase width. A collaborator tested *chopped* pulses: eight pulses with a phase width of 25 μ s at a pulse rate of 1500 pps and compared the response to the response to a single pulse with 200 μ s phase width. The eye movement response was marginally larger for the latter, but the shorter phase width would facilitate recording (D. Jiang, *pers. comm.*, February 2013).

These first measurements contained stimulation artifact due to the proximity of stimulation and recording electrodes on the electrode array. The masker-probe technique was applied and yielded VECAP with negative and positive waves similar to ECAPs in the literature. VECAP recordings presented herein and literature are difficult to compare to literature due to the different electrode arrays and their surgical placement. Latencies in our VECAP recordings were shorter with the negative and positive waves occurring before 200 μ s and at approx. 230 μ s, respectively. In literature, negative waves peak between 200-300 μ s and positive waves between 400-600 μ s (Abbas et al., 1999; Nie et al., 2011). This could be due to species and size difference – here guinea pig, literature rhesus monkey or human – and also recording configuration – here bipolar, literature monopolar. The smaller size of the vestibular labyrinth in the guinea pig could explain shorter traveling times for action potentials and thus shorter latencies.

However, from the 42 possible recording combinations, only a few combinations had N-P characteristic. A better understanding of how the VECAP signal is measured with the given electrode array is necessary. Lai and Dillier proposed a two component model for auditory ECAPs to explain different ECAP shapes. More recent models use finite element modeling and computational models of neurons to simulate the electrical stimulation by a vestibular implant (Hayden et al., 2011, Marianelli et al., 2015). These models could be modified to include VECAP recording.

The masker-probe technique, however, has one drawback. The application of a masker pulse would have an undesired physiological response such as eye movement. A probe artifact template and a sub-threshold template were

tested as alternatives. The probe artifact template, learned with data from another day, was a good proxy for the full masker-probe technique. This was visible in the individual VECAP measurements and also in the amplitude growth function. The sub-threshold template, however, returned only a sharp positive wave. This indicated that measurements with 'sub-threshold' pulse amplitude already contained some compound action potential, although no eye movement response was observed. This was further emphasized by the shape of the sub-threshold template with the negative and positive waves (Fig. 5.4F). For VECAP we would not recommend using sub-threshold artifact reduction.

Comparison to other recording modalities Other electrophysiological tools exist to measure more directly in single afferents (peripherally or centrally) or to measure responses with longer latency such as vestibular evoked myogenic potentials.

Single unit recordings would provide the highest temporal and spatial resolution, but would require, for instance, needle or tungsten microelectrodes and their implantation for chronic measurements. Furthermore, these recordings would require more extensive analysis (e.g., spike sorting) than the minimum and maximum search for VECAP (with some time constraints).

Vestibular evoked myogenic potentials are used clinically to assess otolith function. They are evoked by short pulses of air-conducted sound, electrical stimulation or bone-conducted vibration and measured with surface electrodes placed on muscles (Rosengren et al., 2010). Since it is a myogenic response, latencies are in the range of 10–30 ms. In comparison, VECAPs occur within one millisecond and, more conveniently, they can be recorded with the electrode array that is also used for stimulation.

5.5 SUMMARY

We successfully recorded VECAP with a custom, double-sided electrode array in one guinea pig. The masker-probe paradigm could be substituted with a probe artifact template to avoid physiological responses to the masker pulse. Furthermore, VECAPs may have a good utility, i.e. they may provide additional, useful information without the requirement for extra special acquisition hardware.

6

INVESTIGATING VECAP AND VOR CORRELATION

Abstract Vestibular implant studies with animal models and human subjects demonstrated activation of the vestibular-ocular reflex. The reflex response was then used to benchmark vestibular function. Additional objective metrics, besides the VOR response, could prove useful. Here, we measured peripheral neural function through vestibular electrically evoked compound action potentials.

Guinea pigs were instrumented with a multi-site electrode array – capable of stimulation and recording – in one semicircular canal. VECAP was measured in response to single pulses, pulse trains and during acute continuous stimulation (25 µs/phase for all cases). The negative wave to positive wave voltage (N-P voltage) was extracted as feature. VOR responses were measured with the search coil implanted in the animals' eyes.

In all subjects, correlation of peak eye velocity and N-P voltage in response to single pulses revealed a piecewise linear pattern and could represent a vestibular threshold. In response to pulse trains, N-P voltage was slightly reduced, but not significantly, while PEV increased only for up to five pulses. After adaptation to acute continuous stimulation, pulse amplitude steps elicited bidirectional VOR responses; there were also bidirectional changes in N-P voltage in one guinea pig.

Our findings revealed that N-P voltage reflects PEV and thus might be exploited in a vestibular implant for automatic fitting, and pending more research, also in a closed-loop VI.

6.1 INTRODUCTION

As described in Chapter 2, VIs in animal models have been using a motion sensor fixed to the subject to detect head rotation. A controller then processes that information and applies motion-modulated, pulsatile stimulation through electrodes implanted in the inner ear. The modulation gain is open-loop, i. e. not automatically adapted during implant use. Stimulation efficacy is assessed by recording the VOR response.

Further advances could be achieved by introducing a closed-loop VI with VECAPs as feedback signal. Exploiting VECAP's short latency (1 ms), stimula-

tion efficacy could be assessed in real-time and electrical stimulation adjusted accordingly to achieve a desired VOR response (Fig. 6.1A, information flow representation). The previous Chapter 5 reported VECAP recording with a custom, double-sided electrode array (Poppendieck et al., 2014). Here, these recordings were coupled with VOR responses that would facilitate VOR prediction from VECAP. The controller could then compare predicted VOR with a reference VOR trajectory derived from head motion (Goldberg et al., 2012).

This chapter investigated the correlation of VECAP and VOR in response to (i) single pulses, (ii) pulse trains, (iii) during continuous baseline stimulation. This sequence of experiments allowed us to learn more about VECAP and move towards a typical scenario for a VI operating with a baseline stimulation at a superphysiological baseline pulse rate (e.g., 200 pps). The baseline stimulation facilitated pulse modulation for bidirectional VOR responses. Results of these studies help identify the VECAP-VOR correlation, which is essential for VOR prediction.

6.2 MATERIALS

6.2.1 *Animal Preparation*

The institutional animal care and use committee approved all experiments. Four male guinea pig were prepared with three surgeries (cf. Chapter 5). First, a container for connectors, wires and optional stimulation circuitry ('headcap') as well as a fiberglass-composite structure ('headbolt') were fitted to the animal's skull. Second, a 3-turn stainless steel eye coil was inserted into the left eye. Thirdly, a double-sided electrode array with eight stimulation sites was implanted in the left lateral canal. During surgery, the array's position was checked with a portable stimulator and by monitoring eye movement. A wire electrode was inserted into the neck muscle as remote return electrode.

6.2.2 *General Experimental Setup and Analysis*

A MED-EL Research Interface Box II (RIB2, Innsbruck, Austria) was used for stimulation and recording. It was connected to the implanted electrode array through a transmission coil, PULSAR cochlear implant and a subcutaneous cable to connect implant and electrode array. Scripts with stimulation sequences and recording parameters were programmed in Matlab (MathWorks, Natick, MA, USA). After inspecting all electrode sites on the electrode array,

one site and the remote return were chosen for stimulation (typically the one with the strongest VOR response). For VECAP measurements, two other sites on the array had to be used. The two sites, whose recordings in preliminary tests exhibited both negative and positive waves, were selected. Chapter 5 describes the procedure in more detail. Additionally, before each experiment, the impedances of all electrode sites were measured with the RIB2 and the subject was head-fixed in a dark room during experiments.

Stimulation pulses had a phase width of 25 μ s and 2.1 μ s phase gap (minimum by RIB2). Stimulation artifact was reduced with the masker-probe technique. Masker and probe pulses were 300 μ s apart, i.e., the probe pulse was applied during the absolute refractory period. The masker amplitude was 20 current units larger than the probe amplitude (current units are a proprietary unit used in the RIB2, 1 cu \sim 1 μ A). VECAP response were averaged over 30 iterations in Matlab.

For VOR measurements, the subject was held in an electromagnetic field (Gong and Merfeld, 2000) and the implanted steel coil was connected to a National Instruments DAQ card (Austin, TX, USA). A LabVIEW program measured induced currents in the coil and computed eye position with a sampling rate of 300 kHz and a low-pass RC filter with a 3 kHz cut-off. Another software 4th order Butterworth filter was applied (low-pass, 500 Hz cut-off). Eye movement velocity was differentiated from position using the Matlab `filter` command. VOR responses were averaged over 60 iterations in Matlab.

For correlation and comparison purposes, VECAP and VOR responses were normalized to the largest N-P voltage and peak eye velocity (PEV), respectively, for a given subject and experiment (single pulse, pulse trains or baseline stimulation).

6.2.3 *Specific stimulation and recording paradigms*

Figure 6.1B-D illustrate the three experiments. VOR and VECAP were both measured for all experiments.

Single pulses VECAP and VOR responses were recorded to at least seven different pulse amplitudes linearly spaced between 0 μ A and the maximum current level limited by the compliance voltage of the stimulator (Fig. 6.1B). VECAP and VOR were separately recorded since the electromagnetic field for VOR recording would have affected the VECAP recording. Maximum levels, stimulation and recording electrodes for each subject are listed in Table 6.1.

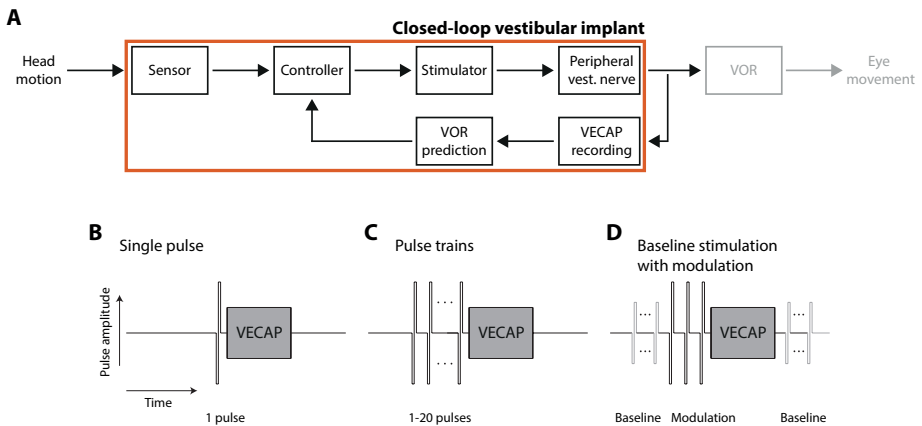


Figure 6.1: Closed-loop VI concept for a vestibular implant and VECAP test paradigm. (A) An expansion of the scheme in Fig. 2.2 with a closed-loop. For gaze stabilization, head motion would entail a counteracting and compensating VOR response. A VOR reference trajectory. VECAP recording could be utilized to predict VOR response and adjust stimulation settings to reduce error. (B-D) VECAP and VOR were recorded to single pulses, pulse trains (1, 2, 5, 10 and 20 pulses) and with baseline stimulation.

Pulse trains Prior to the application of the pulse trains, the subject was not adapted to any baseline stimulation. First, VOR was recorded to pulse trains of 1, 2, 5, 10 or 20 pulses at a pulse rate of 250 pulses per second (pps). These trains consisted only of probe pulses with a constant pulse amplitude at 60% of the maximum level. Afterwards the coil system was turned off for VECAP recording.

VECAP was recorded to the same pulse trains. The set of pulse trains was repeated three times to record responses to probe, marker-probe and marker pulses (Fig. 6.1C).

VECAP during baseline stimulation Subject 3 was freely moving in a small cage, in contrast to the other head-restrained experiments. VOR was not recorded and the search coil system was off. Baseline stimulation was turned on for four 30-minute periods. Pulse rate was 250 pps, current amplitude 160 cu. Other pulse settings were unchanged. VECAP was recorded in intervals of three minutes with the full marker-probe paradigm. A complete recording cycle of 30 iterations for probe, marker-probe and marker took 765 ms, i. e. no baseline stimulation was applied during that period.

VECAP to pulse amplitude steps after adaptation to baseline stimulation This experiment shared some similarities with the study reported in Chap. 4. Sub-

Table 6.1: Stimulation and recording settings for VECAP-VOR study

Subject	Lower threshold [cu]	Maximum level [cu]	Stimulation electrode site	Recording electrode sites
Sub1	420	720	4	8-5
Sub2	200	600	2	1-3
Sub3	190	315	2	4-7
Sub4	200	450	7	1-6

Stimulation was monopolar in all cases, the return electrode was an electrode in the neck musculature.

The second electrode served as recording ground.

Subjects 3 and 4 were subjected to baseline stimulation for 12 minutes (Saginaw et al., 2010) with the baseline pulse amplitude at 50% of the maximal level. Afterwards five pulses at a different pulse amplitude (lower or higher than baseline pulse amplitude) were applied and the responses recorded. VECAP and VOR were again recorded separately (Fig. 6.1D).

6.3 RESULTS

6.3.1 VECAP-VOR Correlation to Single Pulses

VOR responses were measured to the probe pulse with different amplitudes ranging from 0 to the maximum pulse amplitude. Figure 6.2A illustrates an example of VECAP after processing with the masker-probe technique. Figure 6.2B shows an example of averaged horizontal VOR velocity to 600 μ A stimulation in subject 1 (Sub1). Stimulation of the horizontal canal evoked predominantly horizontal VOR response with only small, negligible vertical VOR (ratio ca. 4:1; we therefore focused on horizontal VOR responses for the remainder of this chapter). Velocities peaked at about 7 ms after stimulation onset, which is typical for this species.

Figure 6.2C relates normalized PEV to pulse amplitude for all four subjects. They all revealed a piecewise linear pattern with a marked increase in PEV beyond a certain N-P voltage. Up to that inflection point, N-P voltage increased, while no or little VOR response was evoked. The inflection points were different for all subjects: 0.78, 0.87, 0.66 and 0.5 for Sub1 through Sub4, respectively. Piecewise linear fits to the data were good with $r^2 > 0.75$, and best for Sub4 with 0.969.

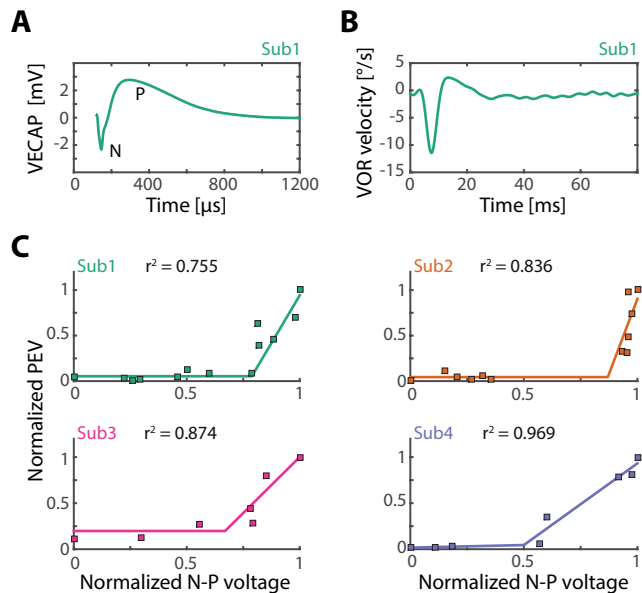


Figure 6.2: VECAP-VOR correlation to single pulses. (A) VECAP recording in Sub1 at $600 \mu\text{A}$ had clear N and P waves. (B) The horizontal VOR velocity to the same single pulse as in (A). The negative velocity indicated eye movement to the right. (C) VECAP-VOR correlation to single pulses for all four subjects. The piecewise linear pattern was evident in all subjects. However, they had different inflection points and slopes.

6.3.2 VECAP-VOR Correlation to Pulse Trains

The time course of eye velocity for Sub3 and for different pulse numbers are shown in Fig. 6.3A. PEVs occurred approx. 8 ms after the end of the pulse train for 1 and 2 pulses (10 and 12.5 ms, respectively). For the other cases, velocity peaked before the end of the train (e.g., at 15 ms for 10 pulses). After the peak, velocity returned to zero with a small negative overshoot for 1 and 2 pulses. For 5 pulses, velocity decreased rapidly with the end of the train. For 10 and 20 pulses, velocity declined slowly first and then rapidly with the end of the train (inflection points at 40.8 and 81.8 μ s, respectively).

PEV increased with pulse number up to 5 pulses with a gain less than unity (normalized PEV in Fig. 6.3B). Specifically, PEV for 5 pulses was 3.6 times larger than PEV for 1 pulse. For 10 and 20 pulses, PEV did not increase further and was similar to PEV for 5 pulses.

Normalized N-P voltage of VECAP is shown in Fig. 6.3C. N-P voltage was highest after 1 pulse. It then trended down up to 5 pulses and remained relatively unchanged for more pulses. The differences in N-P voltage were not significant (2-sample Kolmogorov-Smirnov test, $p > 0.47$ for Sub3). Latencies for the negative wave were constant at 150 μ s after stimulation onset. Also the latencies for the positive wave remained stable at ca. 250 μ s (not shown).

6.3.3 VECAP-VOR Correlation with Baseline Stimulation

In Fig. 6.4A, the N-P voltage showed an increasing trend with time, but the differences were insignificant (2-sample KS-test, $p > 0.05$). Latencies for N and P waves did not change significantly over 30-minutes. P wave latency oscillated between 220 and 240 μ s, while N wave latency was constant at 122.5 μ s.

After adaptation to acute continuous stimulation, subjects were head restrained to measure both VECAP and VOR. While continuing baseline stimulation, brief pulse trains of different pulse amplitude were applied. Specifically, five pulses were applied with lower or higher pulse amplitude than baseline pulse amplitude. These steps elicited bidirectional VOR responses in Sub3, i.e., left or right. In Sub4, higher pulse amplitude evoked a clear directional VOR response, while lower pulse amplitude had no effect. Figure 6.4C shows the correlation between VECAP and PEV. The linear fit was good for Sub3, although only four pulse amplitude steps were tested ($r^2 = 0.987$). For Sub4, r^2 was 0.471 due to the weak VOR response for lower pulse amplitudes.

The recording time of 765 ms every three minutes should have had no major impact on the nerve state (the recording delivered 90 pulses in the same period

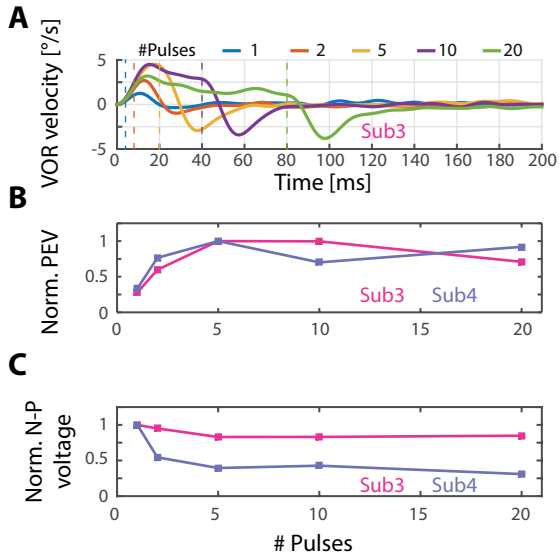


Figure 6.3: VECAP-VOR correlation to pulse trains. (A) VOR velocity in Sub3 for different pulse trains with 1 to 20 pulses. The vertical dashed lines mark the end of the corresponding pulse train. (B) Normalized PEV for Sub3 and Sub4. Both had the same trend; an increase of PEV until five pulses and then a plateau. (C) Normalized N-P voltage in the same subjects. The highest value occurred after a single pulse and declined insignificantly until five pulses.

that 191 baseline pulses would be expected). Total recording time constituted 8.4 s or less than 0.5% of stimulation time.

6.4 DISCUSSION

6.4.1 VECAP-VOR Correlation

We studied the correlation between VECAP and VOR response to single pulses, pulse trains and with baseline stimulation. VECAPs in the literature have been proposed as intraoperative tool for electrode placement and was successful in animal instrumentation (Nie et al., 2011). One group also presented an abstract at the meeting of the Association of Research in Otolaryngology (Dai et al., 2012b), reporting VECAP and VOR responses to single pulses in a rhesus monkey, similar to the ones presented herein.

Single pulses The single pulse responses were the first step towards VOR prediction with VECAP and showed a piecewise linear pattern. For below threshold pulse amplitudes, N-P voltage increased, while no VOR response

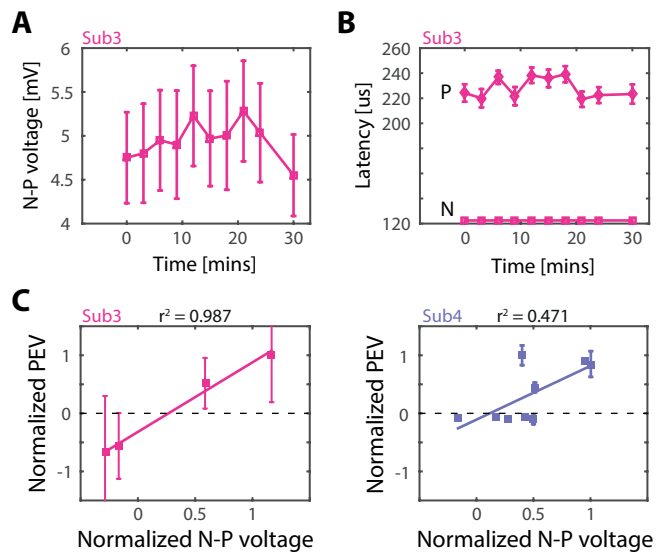


Figure 6.4: VECAP-VOR correlation with baseline stimulation. (A)-(B) VECAP recording in Sub3 at baseline stimulation every 3 minutes over 30 minutes. Neither N-P voltage nor N or P latencies did change significantly in magnitude . (C) After continuous baseline stimulation, brief pulse trains of 5 pulses with lower or higher pulse amplitude were applied to evoke bidirectional responses and record according VECAP. Sub3 showed bidirectional VOR responses and a linear function was fitted to the data. Sub4 showed only VOR responses to pulse trains with higher than baseline pulse amplitude and a fit had low r^2 value. (Error bars in Sub4 were smaller than the marker.)

was evoked. For above threshold pulse amplitudes, PEV increased together with N-P voltage. The pattern was expected: We anticipated VECAP to gauge vestibular nerve activation before any visible VOR response. However, it is not certain what the exact mechanism is. One hypothesis is that VOR onset requires a minimum amount of nerve activity or a minimum number of action potentials which would represent a detection threshold. A second hypothesis is that below threshold stimulation preferentially recruits irregular afferents because of their higher sensitivity to galvanic electrical stimulation. Stronger pulse amplitudes then recruit regular afferents that play a more important role in the VOR response than irregular afferents (Minor and Goldberg, 1991). If the second hypothesis were true, and if one could specifically stimulate regular afferents, then this could lead to a more efficient vestibular implant. A combination of VECAP, single unit and VOR recording could address this question.

Clinically more relevant, the inflection points of the piecewise liner fits could be used for subject-specific automatic threshold estimation. The points of the fits and the slopes of the rising part of the pattern were different for each subject. This was due to the different dynamic ranges, i. e. the difference between lower, vestibular threshold and maximal level (Table 6.1). A small range would result in an inflection at high normalized N-P voltage and higher slope, such as with Sub2 (Fig. 6.2C). These dynamic ranges are difficult to control for and depend on precise electrode placement, the individual tissue-electrode reaction and, in patients, also on etiology and status of the nerve. (In our animal model, vestibular pathology was induced by electrode insertion into the ampulla and rendering the canals insensitive to rotation.) Ideally one would strive for a maximum possible dynamic range to have more available pulse amplitudes.

Pulse trains Pulse trains generated larger VOR responses than single pulses. This is relevant since VOR responses to single pulses are likely to be insufficient for daily activity (e. g., for Sub1 PEV -11.5 °/s or 0.05°eye movement). However, our findings revealed that PEV only increased for pulse trains up to five pulses.

More tests will be required to explain the phenomenon. Tests herein were performed at a pulse rate of 250 pps and higher pulse rates may evoke higher PEV. In fact, in a singular test we applied 3000 pps in Sub3 (D. Jiang, *pers. comm.*, February 2013). We evoked higher PEV and the maximum was obtained with 20 pulses. One possible explanation might be eye muscle fatigue. Muscle fibers are able to exert maximum force (i. e., maximum acceleration) in response to the first pulse(s), but are not able to sustain that force level afterwards because

of the preceding muscle twitch and insufficient recovery time. For instance, twitch time in monkeys was measured between 6 and 8 ms (Fuchs and Luschei, 1971) and would fit the observation that PEV for 5, 10 and 20 pulses at 250 pps occurred around 10 ms.

N-P voltage was stable and did not change significantly for different pulse trains. Although differences were insignificant, the downward trend from 1 to 5 pulses could be viewed as a transition from an impulse response to a steady state. The stable latencies for N and P waves further indicate that neither the shape of VECAP changed with pulse number. This was no surprise. From the previous chapter, we learnt that VECAP to a single pulses recovered within 1 ms. Similarly, VECAPs in rhesus monkey returned to baseline within that time (Nie et al., 2011). Here, the pulses were applied every 4 ms, which gave sufficient recovery time.

Baseline stimulation VECAP was recorded in three minute intervals during 30 minutes of continuous stimulation. No significant change in N-P voltage was observed as expected. VECAP recovers to baseline within 1 ms, therefore continuous stimulation at 250 pps (a pulse every 4 ms) should not affect VECAP *at this time scale*. Long-term continuous stimulation over one week or longer could initiate changes at the electrode-tissue interface that in turn could alter electrode impedance and VECAP (Phillips et al., 2014).

Applying pulse amplitude steps lower or higher than baseline pulse amplitude successfully evoked bidirectional VOR responses in Sub3. In Sub4, only higher than baseline pulse amplitudes evoked a unidirectional. A linear function was fitted to the data and could be used to estimate VOR from VECAP. Though the fit had a high r^2 value for Sub3, VOR variance was large (on average 38.3% of mean). In Sub4, variance was low, but r^2 was less than 0.5. We had hoped to see a linear relation between N-P voltage and PEV, but did not expect standard deviation as large as observed. The results in Sub4 might be related to a device problem in the cochlear implant that we noticed shortly after and could explain why lower than baseline pulse amplitudes did not evoke a VOR response.

6.4.2 Closed-loop Control for Vestibular Implant

In the proposed closed-loop VI, the N-P voltage from VECAP recordings would be utilized to predict the VOR response output and to adjust stimulation parameters to reduce output error. VECAP has the advantage of a shorter latency (1 ms) than the optokinetic system that only uses visual feedback (5-10 ms).

Our findings can be regarded as first stepping stone and are promising in that regard. However, to achieve a closed-loop VI requires more research and testing. First, we have related N-P voltage only to PEV, a parameter that does not contain information about the time course of the VOR response. To follow a reference VOR trajectory, a controller could view that trajectory as sequence of PEVs.

Second, PEV is also dependent on the number of applied pulses. Since VECAP did not change significantly with the number of pulses, the number and likely also eye muscle fatigue would have to be taken into account for PEV. This parameter is known to the controller.

Third, the prediction is dependent on the baseline stimulation. It facilitated bidirectional VOR responses. The computed linear fit may shift with baseline pulse amplitude and would have to be learned specifically for the applied baseline pulse amplitude.

Fourth, the prediction with VECAP is currently only compatible with pulse amplitude modulation. Pulse rate modulation would yield different and lower VOR responses (cf. Chap. 4), but would not change VECAP output that is driven by pulse amplitude. One approach would be to additionally include the pulse rate in the prediction, also a parameter known to the controller.

Finally, the variance in both VECAP and VOR was substantial. The variance in VECAP is related to an offset in the recording unit of the cochlear implant. It could be reduced with better internal settings we had no access to. The variance in VOR is likely related to the small PEVs evoked (ca. 5 °/s) and thus small signal-to-noise ratio. More typically required PEV would be around 30 °/s (Merfeld et al., 2007; Perez-Fornos et al., 2014). To achieve these PEVs, higher stimulation rates greater than 500 pps are necessary as longer phase width would impede VECAP recording. However, high pulse rates may entail other effects such as desynchronization of afferents that have not been studied in the vestibular system, but to some extent in the cochlear system (Litvak et al., 2003).

6.5 SUMMARY

VECAP and VOR responses were recorded to single pulses, pulse trains and with baseline stimulation. Responses from single pulses could be clinically used for automatic threshold estimation which would be more time efficient than the current practice of applying stimulation - inquiring patient - increasing stimulation - inquiring patient etc. Though we found correlations between the responses, they would not be sufficiently robust for a closed-loop VI for

6.5 SUMMARY

the time being. Responses to pulse trains and with baseline stimulation were encouraging, but also revealed that a closed-loop VI will require more research and testing.

Part III
CONCLUSIONS

SUMMARY AND OUTLOOK

Our sixth sense for balance plays a vital role in everyday life. For instance, the vestibulo-ocular reflex stabilizes our gaze and allows us to read messages on our phones while we are walking. Bilateral loss of vestibular function disrupts more than gaze stabilization and significantly reduces quality of life. Currently a vestibular implant is the most promising rehabilitation option for affected patients.

Within the European-US project CLONS, BVL patients were instrumented with modified cochlear implants that provided independent electrode sites for vestibular stimulation. In Part I, we examined four patients acutely with pulse rate and pulse amplitude modulation and we strongly recommend PAM as stimulation paradigm for initial implant activation. In Part II, we pursued a more risky and bold goal of CLONS and made first steps towards a closed-loop VI with VECAP as feedback signal. Results of VECAP-VOR correlation were encouraging, but will require future effort.

SCIENTIFIC CONTRIBUTIONS

Regarding **Aim 1** of identifying efficient electrical stimulation paradigms for VI activation, we programmed a real-time research platform that can interface with any MED-EL cochlear implant with latencies less than 10 ms. Standard clinical tools, such as the company's Research Interface Box or Diagnostic Interface Box, have too large a latency and cannot interface with an external sensor such as a rotation sensor. The research platform could be also used for other scenarios where implanted electrodes in other parts of the body are activated by a cochlear implant.

The study design for Chapter 4 injected identical charge with PAM and PRM and our experimental results and model simulations revealed that PAM evoked stronger responses than PRM. It is a clinically relevant finding that PAM is more efficient than PRM for VI activation. Surprisingly, our findings cast strong doubts on the common notion that same charge equates to same number of evoked action potentials which in turn evoke the same eye movement response. Specifically, the model revealed different ensemble firing rates for charge-equivalent PAM and PRM (higher for PAM). And even assuming identi-

SUMMARY AND OUTLOOK

cal ensemble firing rates for PAM and PRM, PAM taps afferents with stronger synaptic weights than PRM leading to stronger eye movement responses.

Regarding **Aim 2** of characterizing VECAPs in animal models, we reported VECAPs in correlation with VOR responses for different stimulation scenarios. Techniques were described to record and reduce artifact with a multi-site, double-sided electrode array. The techniques could be useful if the electrode array were to be deployed in other cases.

Second, we introduced the concept of a closed-loop VI with VECAP as feedback signal. A provisional US patent application for a closed-loop VI had been filed, but was not further pursued because of electrode issues and because results (from one guinea pig at the time) were not sufficiently compelling. However, by pursuing the audacious goal of a closed-loop VI, we found other opportunities for clinical applications of VECAP such as threshold estimation.

OUTLOOK

We are now on the cusp of a major step towards commercial VIs. In two to three years, the first patients could use a chronically active VI *outside* a controlled laboratory environment. Some obstacles remain. Besides regulatory approval, a motion sensor has to be fixed to the subject's head and the processing unit of the cochlear implant has to be adapted to accommodate vestibular stimulation. These chronic tests will reveal how the subject and the subject's central pathways will adapt to the stimulation and could lead to the first generation of commercial VIs.

We promote VECAP as instrument to improve the use of VIs and future VI performance in the medium and long term (10 years). It has already been suggested as tool for electrode placement during surgery. A medium term step would be to include VECAP for implant fitting post surgery and also during regular follow-ups. This would be more efficient than the currently laborious protocol. In fact, this year we have started a collaboration with an industrial partner (MED-EL) to record VECAPs in human patients. The results will determine whether VECAPs can be recorded with the current vestibular implants. The outcome will also outline possible modifications for better VECAP recording and discuss steps to put VECAPs into clinical use. In the long term, implementing VECAP as feedback signal for a closed-loop VI could boost implant performance by providing a consistent input to the VOR and other pathways.

SUMMARY AND OUTLOOK

The vestibular implant will provide BVL patients with a treatment option to restore vestibular function and quality of life. With the words of Immanuel Kant, their sense of balance should not err anymore.

BIBLIOGRAPHY

- Abbas P, Brown C, Shallop J, Firszt J, Hughes M, Hong S, and Staller S. Summary of results using the nucleus CI24M implant to record the electrically evoked compound action potential. *Ear and Hearing* 20: 45-59, 1999.
- Andreou C, Pahitas Y, and Georgiou J. Bio-Inspired Micro-Fluidic Angular-Rate Sensor for Vestibular Prostheses. *Sensors* 14: 13173-13185, 2014.
- Angelaki DE, and Cullen KE. Vestibular system: The many facets of a multimodal sense. *Annual Review of Neuroscience* 31: 125-150, 2008.
- Arnold DB, and Robinson DA. The oculomotor integrator: testing of a neural network model. *Experimental Brain Research* 113: 57-74, 1997.
- Aw S, Haslwanter T, Halmagyi G, Curthoys I, Yavor R, and Todd M. Three-dimensional vector analysis of the human vestibuloocular reflex in response to high-acceleration head rotations .1. Responses in normal subjects. *Journal of Neurophysiology* 76: 4009-4020, 1996.
- Bahmer A, Peter O, and Baumann U. Recording and analysis of electrically evoked compound action potentials (ECAPs) with MED-EL cochlear implants and different artifact reduction strategies in Matlab. *Journal of Neuroscience Methods* 191: 66-74, 2010.
- Baloh RW, and Kerber KA editors. *Clinical Neurophysiology of the Vestibular System*. Oxford University Press, 2011.
- Baumann U, and Nobbe A. The cochlear implant electrode-pitch function. *Hearing Research* 213: 34-42, 2006.
- Brown CJ, Abbas PJ, and Gantz B. Electrically evoked whole-nerve action potentials: Data from human cochlear implant users. *The Journal of the Acoustical Society of America* 88: 1385-1391, 1990.
- Carpaneto J, Genovese V, Ghionzoli R, Lewis R, Merfeld D, Sabatini A, and Micera S. Characterization and calibration of a novel 3 axis gyroscope for a vestibular neuroprosthesis (in preparation). *Medical Engineering & Physics*.
- Cohen B, and Suzuki J-I. Eye movements induced by ampullary nerve stimulation. *American Journal of Physiology – Legacy Content* 204: 347-351, 1963.
- Cohen B, Yakushin SB, and Holstein GR. What does galvanic vestibular stimulation actually activate: response. *Frontiers in Neurology* 3: 2012.
- Constantinou TG, Georgiou J, and Toumazou C. A Partial-Current-Steering Biphasic Stimulation Driver for Vestibular Prostheses. *Biomedical Circuits and Systems, IEEE Transactions on* 2: 106-113, 2008.
- Cremer PD, Halmagyi GM, Aw ST, Curthoys IS, McGarvie LA, Todd MJ, Black RA, and Hannigan IP. Semicircular canal plane head impulses detect absent function of individual semicircular canals. 1998, p. 699-716.
- Cullen KE. The neural encoding of self-motion. *Current Opinion in Neurobiology In Press, Corrected Proof: -*, 2011.
- Curthoys IS. Vestibular compensation and substitution. *Current Opinion in Neurology* 13: 27-30, 2000.
- Dai C, Ahn JH, Fridman G, Rahman MA, and Della Santina CC. Electrically-evoked Compound Action Potentials and 3D Vestibulo-ocular Reflex Are Correlated to Each Other and to Electrode

BIBLIOGRAPHY

- Position in Rhesus Monkeys Using a Multichannel Vestibular Prosthesis. In: 35th MidWinter Meeting Association of Research in Otolaryngology. San Diego: 2012.
- Dai C, Fridman G, Chiang B, Davidovics N, Melvin T-A, Cullen K, and Della Santina C. Cross-axis adaptation improves 3D vestibulo-ocular reflex alignment during chronic stimulation via a head-mounted multichannel vestibular prosthesis. *Experimental Brain Research* 1-12, 2011.
- Davidovics N, Fridman G, and Della Santina C. Co-modulation of stimulus rate and current from elevated baselines expands head motion encoding range of the vestibular prosthesis. *Experimental Brain Research* 218: 389-400, 2012.
- Davidovics N, Rahman M, Dai C, Ahn J, Fridman G, and Della Santina C. Multichannel Vestibular Prosthesis Employing Modulation of Pulse Rate and Current with Alignment Precompensation Elicits Improved VOR Performance in Monkeys. *JARO* 14: 233-248, 2013.
- Davidovics NS, Fridman GY, Chiang B, and Della Santina CC. Effects of Biphasic Current Pulse Frequency, Amplitude, Duration, and Interphase Gap on Eye Movement Responses to Prosthetic Electrical Stimulation of the Vestibular Nerve. *IEEE Transactions on Neural Systems and Rehabilitation Engineering* 19: 84 -94, 2011.
- Della Santina CC, Migliaccio AA, and Patel AH. A multichannel semicircular canal neural prosthesis using electrical stimulation to restore 3-D vestibular sensation. *IEEE Transactions on Biomedical Engineering* 54: 1016-1030, 2007.
- Eatock RA, and Songer JE. Vestibular Hair Cells and Afferents: Two Channels for Head Motion Signals. *Annual Review of Neuroscience* 34: 501-534, 2011.
- Fetter M, and Dichgans J. Vestibular neuritis spares the inferior division of the vestibular nerve. 1996, p. 755-763.
- Fridman GY, Davidovics NS, Dai C, Migliaccio AA, and Della Santina CC. Vestibulo-Ocular Reflex Responses to a Multichannel Vestibular Prosthesis Incorporating a 3D Coordinate Transformation for Correction of Misalignment. *JARO-Journal of the Association for Research in Otolaryngology* 11: 367-381, 2010.
- Fridman GY, and Della Santina CC. Progress Toward Development of a Multichannel Vestibular Prosthesis for Treatment of Bilateral Vestibular Deficiency. *The Anatomical Record: Advances in Integrative Anatomy and Evolutionary Biology* 295: 2010-2029, 2012.
- Goldberg J, and Fernandez C. Physiology of Peripheral Neurons Innervating Semicircular Canals of Squirrel Monkey. I. Resting Discharge and Response to Constant Angular Accelerations. *Journal of Neurophysiology* 34: 635-660, 1971a.
- Goldberg J, and Fernandez C. Physiology of Peripheral Neurons Innervating Semicircular Canals of Squirrel Monkey. III. Variations among Units in Their Discharge Properties. *Journal of Neurophysiology* 34: 676-684, 1971b.
- Goldberg JM, Wilson VJ, Cullen K, Angelaki D, Broussard DM, Büttner-Ennever JA, Fukushima K, and Minor L editors. *The Vestibular System: A Sixth Sense*. Oxford University Press, 2012.
- Gong W, Haburcakova C, and Merfeld DM. Vestibulo-Ocular Responses Evoked Via Bilateral Electrical Stimulation of the Lateral Semicircular Canals. *IEEE Transactions on Biomedical Engineering* 55: 2608-2619, 2008.
- Gong W, and Merfeld D. Prototype neural semicircular canal prosthesis using patterned electrical stimulation. *Annals of Biomedical Engineering* 28: 572-581, 2000.
- Grossman GE, Leigh RJ, Abel LA, Lanska DJ, and Thurston SE. Frequency and velocity of rotational head perturbations during locomotion. *Experimental Brain Research* 70: 470-476, 1988.
- Guinand N, Boselie F, Guyot JP, and Kingma H. Quality of life of patients with bilateral vestibulopathy. *The Annals of otology, rhinology & laryngology* 121: 471-477, 2012a.

BIBLIOGRAPHY

- Guinand N, Pijnenburg M, Janssen M, and Kingma H. Visual Acuity While Walking and Oscillopsia Severity in Healthy Subjects and Patients With Unilateral and Bilateral Vestibular Function Loss. *Arch Otolaryngol Head Neck Surg* 138: 301-306, 2012b.
- Guyot J-P, Sigrist A, Pelizzzone M, Feigl GC, and Kos MI. Eye Movements in Response to Electrical Stimulation of the Lateral and Superior Ampullary Nerves. *Annals of Otology Rhinology and Laryngology* 120: 81-87, 2011a.
- Guyot J-P, Sigrist A, Pelizzzone M, and Kos MI. Adaptation to Steady-State Electrical Stimulation of the Vestibular System in Humans. *Annals of Otology Rhinology and Laryngology* 120: 143-149, 2011b.
- Harris DM, Bierer SM, Wells JD, and Phillips JO. Optical nerve stimulation for a vestibular prosthesis. In: Proc SPIE2009, p. 7180-7121.
- Hayden R, Sawyer S, Frey E, Mori S, Migliaccio A, and Della Santina C. Virtual labyrinth model of vestibular afferent excitation via implanted electrodes: validation and application to design of a multichannel vestibular prosthesis. *Experimental Brain Research* 1-18, 2011.
- Hirvonen TP, Minor LB, Hullar TE, and Carey JP. Effects of Intratympanic Gentamicin on Vestibular Afferents and Hair Cells in the Chinchilla. *Journal of Neurophysiology* 93: 643-655, 2005.
- Koehler KR, Mikosz AM, Molosh AI, Patel D, and Hashino E. Generation of inner ear sensory epithelia from pluripotent stem cells in 3D culture. *Nature* 500: 217-221, 2013. Lewis R, Gong W, Ramsey M, Minor L, Boyle R, and Merfeld D. Vestibular adaptation studied with a prosthetic semicircular canal. *Journal of Vestibular Research-Equilibrium & Orientation* 12: 87-94, 2002.
- Lewis RF, Haburcakova C, Gong W, Makary C, and Merfeld DM. Vestibuloocular Reflex Adaptation Investigated With Chronic Motion-Modulated Electrical Stimulation of Semicircular Canal Afferents. *Journal of Neurophysiology* 103: 1066-1079, 2010.
- Lysakowski A, Minor LB, Fernandez C, and Goldberg JM. Physiological identification of morphologically distinct afferent classes innervating the crista ampullaris of the squirrel monkey. 1995, p. 1270-1281.
- Manolis EN, Yandavi N, Nadol JB, Eavey RD, McKenna M, Rosenbaum S, Khetarpal U, Halpin C, Merchant SN, Duyk GM, MacRae C, Seidman CE, and Seidman JG. A Gene for Non-Syndromic Autosomal Dominant Progressive Postlingual Sensorineural Hearing Loss Maps to Chromosome 14q12-13. *Human Molecular Genetics* 5: 1047-1050, 1996.
- Marianelli P, Capogrosso M, Bassi Luciani L, Panarese A, and Micera S. A Computational Framework for Electrical Stimulation of Vestibular Nerve. *Transactions on Neural Systems and Rehabilitation Engineering* PP: PP, 2015 (accepted).
- McKay C, Chandan K, Akhoun I, Siciliano C, and Kluk K. Can ECAP Measures Be Used for Totally Objective Programming of Cochlear Implants? *JARO* 14: 879-890, 2013.
- Merfeld DM, Gong W, Morrissey J, Saginaw M, Haburcakova C, and Lewis RF. Acclimation to chronic constant-rate peripheral stimulation provided by a vestibular prosthesis. *IEEE Transactions on Biomedical Engineering* 53: 2362-2372, 2006.
- Merfeld DM, Haburcakova C, Gong W, and Lewis RF. Chronic vestibulo-ocular reflexes evoked by a vestibular prosthesis. *IEEE Transactions on Biomedical Engineering* 54: 1005-1015, 2007.
- Merfeld DM, and Lewis RF. Replacing semicircular canal function with a vestibular implant. *Current Opinion in Otolaryngology & Head and Neck Surgery* 20: 386-392 310.1097/MOO.1090b1013e328357630f, 2012.
- Minor L, and Goldberg J. Vestibular-nerve inputs to the vestibulo-ocular reflex: a functional-ablation study in the squirrel monkey. *The Journal of Neuroscience* 11: 1636-1648, 1991.
- Nguyen K, Kögler V, DiGiovanna J, and Micera S. Finding Physiological Responses in Vestibular Evoked Potentials. In: IEEE Engineering in Medicine and Biology Conference. Boston, MA, USA:

BIBLIOGRAPHY

2011. Nguyen TA, Ranieri M, DiGiovanna J, Peter O, Genovese V, Perez Fornos A, and Micera S. A Real-Time Research Platform to Study Vestibular Implants With Gyroscopic Inputs in Vestibular Deficient Subjects. *Biomedical Circuits and Systems, IEEE Transactions on* 8: 474-484, 2014.
- Nie K, Bierer SM, Ling L, Oxford T, Rubinstein JT, and Phillips JO. Characterization of the Electrically Evoked Compound Action Potential of the Vestibular Nerve. *Otology & Neurology* 32: 88-97, 2011.
- Nie K, Ling L, Bierer S, Kaneko C, Fuchs A, Oxford T, Rubinstein J, and Phillips J. An Experimental Vestibular Neural Prosthesis: Design and Preliminary Results with Rhesus Monkeys Stimulated with Modulated Pulses. *Biomedical Engineering, IEEE Transactions on* PP: 1-1, 2013.
- Park S, and Hong SK. Angular Rate Estimation Using a Distributed Set of Accelerometers. *Sensors* 11: 10444-10457, 2011.
- Phillips JO, Bierer SM, Ling L, Kaibao N, and Rubinstein JT. Real-time communication of head velocity and acceleration for an externally mounted vestibular prosthesis. In: *Engineering in Medicine and Biology Society, EMBC, 2011 Annual International Conference of the IEEE2011*, p. 3537-3541.
- Poppendieck W, Sossalla A, Krob M-O, Welsch C, Nguyen TAK, Gong W, DiGiovanna J, Micera S, Merfeld D, and Hoffmann K-P. Development, manufacturing and application of double-sided flexible implantable microelectrodes. *Biomedical Microdevices* 1-14, 2014.
- Pozzo T, Berthoz A, and Lefort L. Head stabilization during various locomotor tasks in humans. *Experimental Brain Research* 82: 97-106, 1990.
- Pozzo T, Berthoz A, Lefort L, and Vitte E. Head stabilization during various locomotor tasks in humans. *Experimental Brain Research* 85: 208-217, 1991.
- Robinson DA. The Use of Control Systems Analysis in the Neurophysiology of Eye Movements. *Annual Review of Neuroscience* 4: 463-503, 1981.
- Rosengren SM, Welgampola MS, and Colebatch JG. Vestibular evoked myogenic potentials: Past, present and future. *Clinical Neurophysiology* 121: 636-651, 2010.
- Rubinstein JT, Bierer S, Kaneko C, Ling L, Nie K, Oxford T, Newlands S, Santos F, Risi F, Abbas PJ, and Phillips JO. Implantation of the Semicircular Canals With Preservation of Hearing and Rotational Sensitivity: A Vestibular Neurostimulator Suitable for Clinical Research. *Otology & Neurotology* 33: 789-796 710.1097/MAO.1090b1013e318254ec318224, 2012.
- Saginaw MA, Wangsong G, Haburcakova C, and Merfeld DM. Attenuation of Eye Movements Evoked by a Vestibular Implant at the Frequency of the Baseline Pulse Rate. *Biomedical Engineering, IEEE Transactions on* 58: 2732-2739, 2011.
- Sun D, Ward BK, Semenov Y, Carey J, and Della Santina CC. Bilateral Vestibular Deficiency: Quality of Life and Economic Implications. *JAMA Otolaryngol Head Neck Surg* 140: 527-534, 2014.
- Sun DQ, Rahman MA, Fridman G, Chenkai D, Chiang B, and Della Santina CC. Chronic stimulation of the semicircular canals using a multichannel vestibular prosthesis: Effects on locomotion and angular vestibulo-ocular reflex in chinchillas. In: *Engineering in Medicine and Biology Society, EMBC, 2011 Annual International Conference of the IEEE2011*, p. 3519-3523.
- Suzuki J, Goto K, Tokumasu K, and Cohen B. Implantation of Electrodes near Individual Vestibular Nerve Branches in Mammals. *Annals of Otology Rhinology and Laryngology* 78: 1969.
- Thompson LA, Haburcakova C, Gong W, Lee DJ, Wall III C, Merfeld DM, and Lewis RF. Responses evoked by a vestibular implant providing chronic stimulation. *Journal of Vestibular Research* 22: 11-15, 2012.
- Toreyin H, and Bhatti P. A Field-Programmable Analog Array Development Platform for Vestibular Prosthesis Signal Processing. *Biomedical Circuits and Systems, IEEE Transactions on* 7: 319-325, 2013.

BIBLIOGRAPHY

- Van de Berg R, Guinand N, Guyot J-P, Stokroos R, and Kingma H. The vestibular implant: Quo vadis? *Frontiers in Neurology* 2: 2011.
- Wall I, Conrad, Wrisley DM, and Statler KD. Vibrotactile tilt feedback improves dynamic gait index: A fall risk indicator in older adults. *Gait & Posture* 30: 16-21, 2009.
- Wilson BS. Speech processing strategies. *Cochlear implants: a practical guide* 2: 21-69, 2006. Zierhofer CM. Adaptive sigma-delta modulation with one-bit quantization. *Circuits and Systems II: Analog and Digital Signal Processing, IEEE Transactions on* 47: 408-415, 2000.
- Zingler VC, Weintz E, Jahn K, Mike A, Huppert D, Rettinger N, Brandt T, and Strupp M. Follow-up of vestibular function in bilateral vestibulopathy. *Journal of Neurology, Neurosurgery & Psychiatry* 79: 284-288, 2008.

ACRONYMS

- AGF** amplitude growth function
BVL bilateral vestibular loss
CI cochlear implant
CRIO National Instruments CompactRIO
DRIB direct Research Interface Box
ECAP electrically evoked compound action potential
FPGA field-programmable gate array
ISI interspike interval
GUI graphical user interface
LAN lateral ampullary nerve
MCL most comfortable level
NI National Instruments
OKN optokinetic system
PAM pulse amplitude modulation
PAN posterior ampullary nerve
PEV peak eye velocity
PRM pulse rate modulation
RIB Research Interface Box
RMSE root mean square error
RT real-time
SAN superior ampullary nerve

Acronyms

scc semicircular canal

THR lower, vestibular threshold

VECAP vestibular electrically evoked compound action potential

VI vestibular implant

VN vestibular nuclei

VOR vestibulo-ocular reflex

CURRICULUM VITAE

Name Thuy Anh Khoa Nguyen

Date of birth August 18th, 1985 in Hanoi, Vietnam

Education

05/2010– Doctoral student at Automatic Control Lab, ETH Zurich

01/2013– Visiting doctoral student at Translational

Neural Engineering Lab, EPF Lausanne

10/2004–11/2009 Undergraduate student, degree Diplom-Ingenieur

(Mechatronik), TU Dresden, Germany

09/2007–05/2008 Visiting student at University of Bath, United Kingdom

08/1997–06/2004 Carl-Friedrich-Gauss Gymnasium, Frankfurt (Oder),

Germany

Work

- 02/2010–03/2010 Centre Suisse d'Electronique et
de Microtechnique, Landquart, Switzerland
- 03/2009–01/2010 Student research assistant at
Max Berg Bermann Center for Biomaterials
Dresden, Germany
- 06/2008–10/2008 Student research assistant at Medical-Technical
- 08/2007–09/2007 Laboratories, Charité-Universitätsmedizin
Berlin, Germany
- 10/2008–01/2009 Student teaching assistant
- 10/2005–07/2007 TU Dresden, Germany